

# Approximation of the hydrostatic Navier–Stokes system for density stratified flows by a multilayer model. Kinetic interpretation and numerical solution

E. Audusse<sup>a,b</sup>, M.-O. Bristeau<sup>b</sup>, M. Pelanti<sup>b,c</sup>, J. Sainte-Marie<sup>b,d,\*</sup>

<sup>a</sup>Université Paris 13, Institut Galilée, 99 avenue Jean-Baptiste Clément, 93430 Villetaneuse, France.

<sup>b</sup>INRIA Paris-Rocquencourt, Domaine de Voluceau, 78153, Le Chesnay, France.

<sup>c</sup>Laboratoire National d'Hydraulique et Environnement, EDF R&D, 6 quai Watier, 78401 Chatou, France.

<sup>d</sup>Saint-Venant Laboratory, 6 quai Watier, 78401 Chatou, France.

---

## Abstract

We present a multilayer Saint-Venant system for the numerical simulation of free surface density-stratified flows over variable topography. The proposed model formally approximates the hydrostatic Navier–Stokes equations with a density that varies depending on the spatial and temporal distribution of a transported quantity such as temperature or salinity. The derivation of the multilayer model is obtained by a Galerkin-type vertical discretization of the Navier–Stokes system with piecewise constant basis functions. In contrast with classical multilayer models in the literature that assume immiscible fluids, we allow here for mass exchange between layers. We show that the multilayer system admits a kinetic interpretation, and we use this result to formulate a robust finite volume scheme for its numerical approximation. Several numerical experiments are presented, including simulations of wind-driven stratified flows.

*Keywords:* Hydrostatic Navier–Stokes equations, Saint-Venant equations, Free surface stratified flows, Multilayer system, Variable density, Kinetic scheme.

---

## 1. Introduction

In this paper we present a multilayer Saint-Venant model for the numerical simulation of free surface density-stratified flows over variable topography. We are mainly interested in applications to geophysical water flows such as lakes and estuarine waters, which typically exhibit a significant density stratification related to vertical variations of temperature and chemical composition. In these water bodies effects related to small density gradients may strongly affect the hydrodynamics. Density stratification processes are therefore often important in environmental flows, and in particular they are a key feature in the biogeochemical mechanisms occurring in natural aquatic systems.

The simulation of these flows requires stable, accurate, conservative schemes able to sharply resolve density gradients, to handle efficiently complex topographies and free surface deformations, and to capture robustly wet/dry fronts. In addition, the application to realistic three-dimensional problems demands efficient methods with respect to computational cost. The present work is aimed to build a simulation tool endowed with these properties.

Most of the numerical models in the literature for environmental stratified flows use finite difference or finite element schemes solving the free surface Navier–Stokes equations. We refer in particular to [1, 2, 3, 4] and references therein for a partial review of these methods.

---

\*Corresponding author

*Email addresses:* `audusse@math.univ-paris13.fr` (E. Audusse), `Marie-Odile.Bristeau@inria.fr` (M.-O. Bristeau), `Marica.Pelanti@inria.fr` (M. Pelanti), `Jacques.Sainte-Marie@inria.fr` (J. Sainte-Marie)

Here we propose a different and original approach that uses a multilayer system to approximate the Navier–Stokes equations and a finite volume solution scheme. Our work is an extension to the case of variable density of the multilayer technique with mass exchange introduced in [5] for homogeneous flows. The starting point is the free surface hydrostatic Navier–Stokes system where the density is a function of a transported quantity such as temperature, salinity, pollutant, . . . . The multilayer model is derived by a finite element Galerkin-type vertical discretization of the Navier–Stokes system with piecewise constant basis functions. We use the nomenclature *Saint-Venant system* for the resulting equations since the vertical uniformity assumption and the vertical integration procedure over each layer are the ingredients of the derivation of the classical Saint-Venant equations [6] for shallow water flows. The proposed model presents remarkable differences with respect to classical multilayer models [7, 8, 9, 10], which assume superposed shallow layers of immiscible fluids. In our approach the layer partition is merely a discretization artefact, and it is not physical. Therefore, the internal layer boundaries do not necessarily correspond to isopycnic surfaces. A critical distinguishing feature of our model is that it allows fluid circulation between layers. This changes dramatically the properties of the model and its ability to describe flow configurations that are crucial for the foreseen applications, such as recirculation zones.

With respect to commonly used Navier–Stokes solvers, the appealing features of the proposed multilayer approach are the easy handling of the free surface, which does not require moving meshes (e.g. [11]), and the possibility to take advantage of robust and accurate numerical techniques developed in extensive amount for classical one-layer Saint Venant equations. In particular, here the method for the numerical solution of the multilayer system uses the finite volume kinetic scheme of [12], with an extended hydrostatic reconstruction technique [13] for the treatment of source terms. In contrast with Navier–Stokes solvers, our discretization technique allows easily satisfying properties such as conservation, positivity, well-balancing of source terms (cf. [14]), and handling robustly wet/dry interfaces over variable bottom topography.

Let us also remark that the multilayer model presented here is rather different from the isopycnal coordinate layered models extensively developed in the context of oceanography, e.g. [15, 16]. These models use a primitive equation layered formulation obtained by vertical integration of the Navier–Stokes equations over each Lagrangian layer, and the resulting system is solved by finite difference schemes.

To our knowledge, our multilayer method is a pioneering idea for applications to stratified environmental flows. As a starting work, we consider some simplifications in the physical model, notably the hydrostatic pressure assumption. We do take into account wind surface stress, which is a dominant natural forcing mechanism acting on environmental water flows. However, we neglect surface thermal exchange due to short wave and long wave radiation and evaporative processes. Furthermore, we do not address the issue of turbulence closure, and diffusivity will be assumed constant. Turbulence modeling is a major difficulty for an effective description of diapycnal mixing occurring in realistic flows [3, 17], and it still remains an open problem.

The paper is organized as follows. We start recalling the hydrostatic Navier–Stokes system in Section 2, and the derivation of the multilayer model is illustrated in Section 3. In Section 5 we propose a numerical scheme for the solution of the multilayer system based on a kinetic interpretation, which is detailed in Section 4. Finally, in Section 6, some numerical experiments are presented.

## 2. The hydrostatic Navier–Stokes system with variable density

We begin by considering the two-dimensional hydrostatic Navier–Stokes system [18] describing a free surface gravitational flow moving over a bottom topography  $z_b(x)$ . We denote with  $x$  and  $z$  the horizontal and vertical directions, respectively. The system has the form:

$$\frac{\partial \rho}{\partial t} + \frac{\partial \rho u}{\partial x} + \frac{\partial \rho w}{\partial z} = 0, \quad (1)$$

$$\frac{\partial \rho u}{\partial t} + \frac{\partial \rho u^2}{\partial x} + \frac{\partial \rho u w}{\partial z} + \frac{\partial p}{\partial x} = \frac{\partial \Sigma_{xx}}{\partial x} + \frac{\partial \Sigma_{xz}}{\partial z}, \quad (2)$$

$$\frac{\partial p}{\partial z} = -\rho g + \frac{\partial \Sigma_{zx}}{\partial x} + \frac{\partial \Sigma_{zz}}{\partial z}, \quad (3)$$

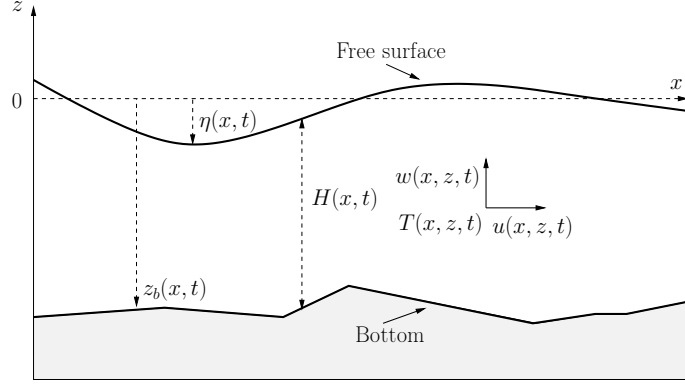


Figure 1: Flow domain with water height  $H(x, t)$ , free surface  $\eta(x, t)$  and bottom  $z_b(x, t)$ .

and we consider solutions of the equations for

$$t > t_0, \quad x \in \mathbb{R}, \quad z_b(x) \leq z \leq \eta(x, t),$$

where  $\eta(x, t)$  represents the free surface elevation,  $\mathbf{u} = (u, w)^T$  the velocity vector and  $g$  the gravity acceleration. The flow height is  $H = \eta - z_b$ , see Fig. 1.

The chosen form of the viscosity tensor is

$$\begin{aligned} \Sigma_{xx} &= 2\mu \frac{\partial u}{\partial x}, & \Sigma_{xz} &= \mu \left( \frac{\partial u}{\partial z} + \frac{\partial w}{\partial x} \right), \\ \Sigma_{zz} &= 2\mu \frac{\partial w}{\partial z}, & \Sigma_{zx} &= \mu \left( \frac{\partial u}{\partial z} + \frac{\partial w}{\partial x} \right), \end{aligned}$$

where  $\mu$  is a dynamic viscosity.

The fluid density  $\rho(x, t)$  is assumed to depend on the spatial and temporal distribution of a given tracer  $T(x, t)$ , namely

$$\rho = \rho(T), \tag{4}$$

and  $T$  is governed by a transport-diffusion equation

$$\frac{\partial \rho T}{\partial t} + \frac{\partial \rho u T}{\partial x} + \frac{\partial \rho w T}{\partial z} = \mu_T \frac{\partial^2 T}{\partial x^2} + \mu_T \frac{\partial^2 T}{\partial z^2}, \tag{5}$$

where  $\mu_T$  is the tracer diffusivity.

**Remark 2.1.** *If we neglect the viscosity terms in the equation (5), we note that the three relations*

$$\begin{aligned} \frac{\partial u}{\partial x} + \frac{\partial w}{\partial z} &= 0, \\ \frac{\partial \rho}{\partial t} + \frac{\partial \rho u}{\partial x} + \frac{\partial \rho w}{\partial z} &= 0, \\ \frac{\partial \rho T}{\partial t} + \frac{\partial \rho u T}{\partial x} + \frac{\partial \rho w T}{\partial z} &= 0, \end{aligned}$$

*are equivalent in the sense that two of them allow recovering the third. Therefore, neglecting the viscosity, the studied system with varying density retains the free divergence property of the constant density model.*

*Nonetheless, at the semi-discrete level (see Prop. 1) and at the full discrete level detailed in Sec. 5, this equivalence no more holds true. For reasons related to the kinetic interpretation and the associated finite*

volume scheme, we prefer to work with equations having the form of time-dependent conservation laws. Thus we will keep the last two equations of the system above in the discretization procedure. This has two consequences. First, our discretization technique is also valid for compressible fluids. Second, at the discrete level our model only satisfies an approximate divergence free condition.

### 2.1. Boundary conditions

The system (1)-(3) is completed with boundary conditions. The outward unit normal vector to the free surface  $\mathbf{n}_s$  and the upward unit normal vector to the bottom  $\mathbf{n}_b$  are given by

$$\mathbf{n}_s = \frac{1}{\sqrt{1 + \left(\frac{\partial\eta}{\partial x}\right)^2}} \begin{pmatrix} -\frac{\partial\eta}{\partial x} \\ 1 \end{pmatrix}, \quad \mathbf{n}_b = \frac{1}{\sqrt{1 + \left(\frac{\partial z_b}{\partial x}\right)^2}} \begin{pmatrix} -\frac{\partial z_b}{\partial x} \\ 1 \end{pmatrix},$$

respectively. We then denote with  $\Sigma_T$  the total stress tensor, which has the form:

$$\Sigma_T = -pI_d + \begin{pmatrix} \Sigma_{xx} & \Sigma_{xz} \\ \Sigma_{zx} & \Sigma_{zz} \end{pmatrix}.$$

#### 2.1.1. Free surface conditions

At the free surface we have the kinematic boundary condition

$$\frac{\partial\eta}{\partial t} + u_s \frac{\partial\eta}{\partial x} - w_s = 0, \quad (6)$$

where the subscript  $s$  indicates the value of the considered quantity at the free surface.

We denote with  $\tau_w$  the surface wind stress, for which the following expression [19] is considered:

$$\tau_w = C_D \frac{\rho_a}{\rho_0} |V_w| V_w. \quad (7)$$

Here  $V_w$  is the wind velocity,  $\rho_a$  the air density,  $\rho_0$  a reference water density, and  $C_D$  the wind drag coefficient (taken as  $C_D = 1.3 \times 10^{-3}$  in the numerical experiments).

Assuming negligible the air viscosity, the continuity of stresses at the free boundary imposes

$$\Sigma_T \mathbf{n}_s = -p^a \mathbf{n}_s + \tau_w \mathbf{t}_s, \quad (8)$$

where  $p^a = p^a(x, t)$  is a given function corresponding to the atmospheric pressure and  $\mathbf{t}_s$  is the unit vector orthogonal to  $\mathbf{n}_s$ .

Relation (8) is equivalent to

$$\mathbf{n}_s \cdot \Sigma_T \mathbf{n}_s = -p^a, \quad \text{and} \quad \mathbf{t}_s \cdot \Sigma_T \mathbf{n}_s = \tau_w.$$

In the following, we will assume  $p^a = 0$ .

#### 2.1.2. Bottom conditions

The kinematic boundary condition at the bottom consists in a classical no-penetration condition:

$$\mathbf{u}_b \cdot \mathbf{n}_b = 0, \quad \text{or} \quad u_b \frac{\partial z_b}{\partial x} - w_b = 0. \quad (9)$$

For the stresses at the bottom we consider a wall law under the form

$$\mathbf{t}_b \cdot \Sigma_T \mathbf{n}_b = \kappa \mathbf{u}_b \cdot \mathbf{t}_b, \quad (10)$$

where  $\mathbf{t}_b$  is a unit vector satisfying  $\mathbf{t}_b \cdot \mathbf{n}_b = 0$ . If  $\kappa(\mathbf{u}_b, H)$  is constant then we recover a Navier friction condition as in [20]. Introducing a laminar friction  $k_l$  and a turbulent friction  $k_t$ , we use the expression

$$\kappa(\mathbf{u}_b, H) = k_l + k_t H |\mathbf{u}_b|,$$

corresponding to the boundary condition used in [21]. Another form of  $\kappa(\mathbf{u}_b, H)$  is used in [22], and for other wall laws the reader can also refer to [23]. Due to thermo-mechanical considerations, in the sequel we will suppose  $\kappa(\mathbf{u}_b, H) \geq 0$ , and  $\kappa(\mathbf{u}_b, H)$  will be often simply denoted by  $\kappa$ .

## 2.2. The Boussinesq assumption

In geophysical water flows density variations are often small. Assuming homogeneous chemical composition, and identifying here  $T$  with the temperature, the equation of state for water bodies can be expressed by the classical relation

$$\rho(T) = \rho_0 (1 - \alpha_T (T - T_0)^2), \quad (11)$$

with  $T_0 = 4^\circ\text{C}$ ,  $\alpha_T = 6.63 \times 10^{-6} \text{ }^\circ\text{C}^{-2}$  (volume coefficient of thermal expansion) and  $\rho_0 = 10^3 \text{ kg m}^{-3}$ . For example, the relative density difference corresponding to two states with temperatures  $T_1 = 25^\circ\text{C}$  and  $T_2 = 10^\circ\text{C}$  is

$$\frac{\rho(25) - \rho(10)}{\rho(10)} \approx 0.0026.$$

Such small differences typically allow justifying the Boussinesq assumption, which consists in considering the density variations only in the gravitational forces. This leads to the following incompressible hydrostatic Navier–Stokes system:

$$\frac{\partial u}{\partial x} + \frac{\partial w}{\partial z} = 0, \quad (12)$$

$$\frac{\partial u}{\partial t} + \frac{\partial u^2}{\partial x} + \frac{\partial uw}{\partial z} + \frac{1}{\rho_0} \frac{\partial p}{\partial x} = \frac{1}{\rho_0} \left( \frac{\partial \Sigma_{xx}}{\partial x} + \frac{\partial \Sigma_{xz}}{\partial z} \right), \quad (13)$$

$$\frac{\partial p}{\partial z} = -\rho g + \frac{\partial \Sigma_{zx}}{\partial x} + \frac{\partial \Sigma_{zz}}{\partial z}, \quad (14)$$

$$\frac{\partial T}{\partial t} + \frac{\partial uT}{\partial x} + \frac{\partial wT}{\partial z} = \nu_T \frac{\partial^2 T}{\partial x^2} + \nu_T \frac{\partial^2 T}{\partial z^2} \quad (15)$$

with  $\nu_T = \frac{\mu_T}{\rho_0}$ . Notice that in (12)–(15) the divergence free condition means a conservation of volume rather than a conservation of mass as in Eqs. (1)–(3).

In the following the Boussinesq assumption is not made, and some remarks about its validity will be given in the discussion of the results of the numerical simulations, see Sec. 6.

## 3. The multilayer system with variable density

In this section we describe the multilayer discretization procedure of the hydrostatic Navier–Stokes system with variable density (1)–(5). For the special case of constant density, a detailed illustration of the derivation of the multilayer Saint-Venant system was given in [5]. Here the presentation is slightly different since we use a vertical space/time Galerkin approximation in order to introduce the layer decomposition. Note that we will focus on the specific aspects arising from the density variations.

### 3.1. Multilayer model derivation

For the sake of simplicity, we omit hereafter the viscous and friction terms of equations (2), (3), (5), (10) (we refer to [5] for the treatment of these terms). Therefore, we start from the hydrostatic free surface Euler equations with varying density.

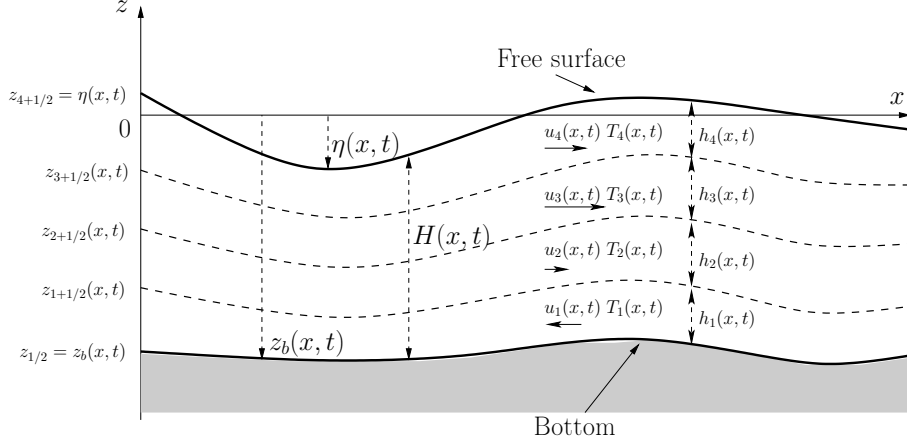


Figure 2: Notations for the multilayer approach.

The interval  $[z_b, \eta]$  is divided into  $N$  layers  $\{L_\alpha\}_{\alpha \in \{1, \dots, N\}}$  of thickness  $l_\alpha H(x, t)$  where each layer  $L_\alpha$  corresponds to the points satisfying  $z \in L_\alpha(x, t) = [z_{\alpha-1/2}, z_{\alpha+1/2}]$  with

$$\begin{cases} z_{\alpha+1/2}(x, t) = z_b(x, t) + \sum_{j=1}^{\alpha} l_j H(x, t), \\ h_\alpha(x, t) = z_{\alpha+1/2}(x, t) - z_{\alpha-1/2}(x, t) = l_\alpha H(x, t), \quad \alpha \in [0, \dots, N], \end{cases} \quad (16)$$

with  $l_j > 0$ ,  $\sum_{j=1}^N l_j = 1$ , see Fig. 2.

Now let us consider the space  $\mathbb{P}_{0,H}^{N,t}$  of piecewise constant functions defined by

$$\mathbb{P}_{0,H}^{N,t} = \{\mathbb{I}_{z \in L_\alpha(x,t)}(z), \quad \alpha \in \{1, \dots, N\}\},$$

where  $\mathbb{I}_{z \in L_\alpha(x,t)}(z)$  is the characteristic function of the interval  $L_\alpha(x, t)$ . Using this formalism, the projection of  $u$ ,  $w$  and  $T$  onto  $\mathbb{P}_{0,H}^{N,t}$  is a piecewise constant function defined by

$$X^N(x, z, \{z_\alpha\}, t) = \sum_{\alpha=1}^N \mathbb{1}_{[z_{\alpha-1/2}, z_{\alpha+1/2}]}(z) X_\alpha(x, t), \quad (17)$$

for  $X \in (u, w, T)$ . The density  $\rho = \rho(T)$  inherits a discretization from the previous relation with

$$\rho^N(x, z, \{z_\alpha\}, t) = \sum_{\alpha=1}^N \mathbb{1}_{[z_{\alpha-1/2}, z_{\alpha+1/2}]}(z) \rho(T_\alpha(x, t)). \quad (18)$$

We have the following result.

**Proposition 1.** *Omitting the viscosity terms, the weak formulation of Eqs. (1)-(3) and (5) on  $\mathbb{P}_{0,H}^{N,t}$  leads to a system of the form*

$$\sum_{\alpha=1}^N \frac{\partial \rho_\alpha h_\alpha}{\partial t} + \sum_{\alpha=1}^N \frac{\partial \rho_\alpha h_\alpha u_\alpha}{\partial x} = 0. \quad (19)$$

$$\begin{aligned} \frac{\partial \rho_\alpha h_\alpha u_\alpha}{\partial t} + \frac{\partial}{\partial x} (\rho_\alpha h_\alpha u_\alpha^2 + h_\alpha p_\alpha) &= u_{\alpha+1/2} G_{\alpha+1/2} - u_{\alpha-1/2} G_{\alpha-1/2} \\ &+ \frac{\partial z_{\alpha+1/2}}{\partial x} p_{\alpha+1/2} - \frac{\partial z_{\alpha-1/2}}{\partial x} p_{\alpha-1/2}, \end{aligned} \quad (20)$$

$$\frac{\partial \rho_\alpha h_\alpha T_\alpha}{\partial t} + \frac{\partial}{\partial x} (\rho_\alpha h_\alpha T_\alpha u_\alpha) = T_{\alpha+1/2} G_{\alpha+1/2} - T_{\alpha-1/2} G_{\alpha-1/2}, \quad (21)$$

$$\alpha \in [1, \dots, N],$$

with  $h_\alpha = l_\alpha H$ . The definitions of  $p_\alpha$ ,  $p_{\alpha+1/2}$ ,  $u_{\alpha+1/2}$ ,  $T_{\alpha+1/2}$ ,  $G_{\alpha+1/2}$  are given in the following (eqs. (27), (28), and (25)).

**Proof.** Using the Leibniz rule, the Galerkin approximation of Eq. (1) on  $\mathbb{P}_{0,H}^{N,t}$  gives the set of equations

$$\frac{\partial \rho_\alpha h_\alpha}{\partial t} + \frac{\partial}{\partial x} (\rho_\alpha h_\alpha u_\alpha) = G_{\alpha+1/2} - G_{\alpha-1/2}, \quad \alpha \in [1, \dots, N], \quad (22)$$

with

$$G_{\alpha+1/2} = \rho_{\alpha+1/2} \left( \frac{\partial z_{\alpha+1/2}}{\partial t} + u_{\alpha+1/2} \frac{\partial z_{\alpha+1/2}}{\partial x} - w_{\alpha+1/2} \right), \quad (23)$$

$$G_{1/2} = G_{N+1/2} = 0. \quad (24)$$

Relations (23) give the mass flux leaving/entering each layer  $\alpha$ , and relations (24) express that the bottom and the top boundaries are interfaces without loss/supply of mass (see the boundary conditions (6), (9)).

Let us note that the layer mass equation (22) cannot be used per se since the layer height  $h_\alpha$  is not an independent variable but it is defined as a part of the total water height  $H(t, x)$ , see relation (16). Nonetheless, using the first condition of (24), one can compute the mass flux  $G_{\alpha+1/2}$  just adding up the equations (22):

$$G_{\alpha+1/2} = \sum_{j=1}^{\alpha} \frac{\partial \rho_j h_j}{\partial t} + \sum_{j=1}^{\alpha} \frac{\partial \rho_j h_j u_j}{\partial x}, \quad \alpha = 1, \dots, N. \quad (25)$$

Then the equation (25) written for  $\alpha = N$  and the second condition of (24) give the equation (19). The need to consider only the global mass equation (19) is related to the fact that we consider a single fluid with varying density, and not several layers of non-miscible fluids as in some other multilayer models [7, 8, 9, 10]. Then it is physically consistent to consider a conservation law for the total mass (flow height), which enables circulation of the fluid between the layers introduced in the discretization process. In the following, we use the formula (25) rather than (23), and thus we have not to define  $\rho_{\alpha+1/2}, w_{\alpha+1/2}$ .

Similarly, the  $\mathbb{P}_{0,H}^{N,t}$ -approximation of the  $x$ -momentum equation (2) leads to (20). Indeed from (3) we can compute

$$p(x, z, t) = g \int_z^\eta \rho dz,$$

and using (18), we have for  $z \in L_\alpha$

$$p(x, z, t) = g \left( \sum_{j=\alpha+1}^N \rho_j h_j + \rho_\alpha (z_{\alpha+1/2} - z) \right).$$

Using the notations

$$p_\alpha = \frac{1}{h_\alpha} \int_{z_{\alpha-1/2}}^{z_{\alpha+1/2}} p(x, z, t) dz, \quad p_{\alpha+1/2} = p(x, z_{\alpha+1/2}, t), \quad (26)$$

we have

$$p_\alpha = g \left( \frac{\rho_\alpha h_\alpha}{2} + \sum_{j=\alpha+1}^N \rho_j h_j \right) \quad \text{and} \quad p_{\alpha+1/2} = g \sum_{j=\alpha+1}^N \rho_j h_j, \quad (27)$$

and applying the Leibniz rule to the pressure term of equation (2) we can write

$$\int_{z_{\alpha-1/2}}^{z_{\alpha+1/2}} \frac{\partial p}{\partial x} dz = \frac{\partial h_{\alpha} p_{\alpha}}{\partial x} - \frac{\partial z_{\alpha+1/2}}{\partial x} p_{\alpha+1/2} + \frac{\partial z_{\alpha-1/2}}{\partial x} p_{\alpha-1/2}.$$

Relation (21) also comes from a Galerkin approximation on  $\mathbb{P}_{0,H}^{N,t}$  of equation (5) and the application of the Leibniz rule.

To complete the definition of equations (20), (21), the quantities  $u_{\alpha+1/2}$ ,  $T_{\alpha+1/2}$ ,  $\alpha = 1, \dots, N-1$ , are defined by using an upwind strategy:

$$v_{\alpha+1/2} = \begin{cases} v_{\alpha} & \text{if } G_{\alpha+1/2} \geq 0, \\ v_{\alpha+1} & \text{if } G_{\alpha+1/2} < 0, \end{cases} \quad (28)$$

for  $v = u, T$ .  $\square$

In conclusion, for a flow height partition into  $N$  layers, the multilayer Saint-Venant system approximating the free surface Euler system is defined by the continuity equation (19), the  $N$   $x$ -momentum equations (20) and the  $N$  tracer equations (21).

### 3.2. Energy

For smooth solutions it is straightforward to obtain an energy equality by multiplying the  $x$ -momentum equation by  $u$ , and by performing the Galerkin approximation on  $\mathbb{P}_{0,H}^{N,t}$ .

For the layer  $\alpha$  we have

$$\begin{aligned} \frac{\partial}{\partial t} E_{sv,\alpha}^N + \frac{\partial}{\partial x} \left( u_{\alpha} \left( E_{sv,\alpha}^N + \frac{g}{2} \rho_{\alpha} h_{\alpha} H \right) \right) = \\ + \left( \frac{u_{\alpha+1/2}^2}{2} + p_{\alpha+1/2} + g z_{\alpha+1/2} \right) G_{\alpha+1/2} - \left( \frac{u_{\alpha-1/2}^2}{2} + p_{\alpha-1/2} + g z_{\alpha-1/2} \right) G_{\alpha-1/2} \\ - p_{\alpha+1/2} \frac{\partial z_{\alpha+1/2}}{\partial t} + p_{\alpha-1/2} \frac{\partial z_{\alpha-1/2}}{\partial t}, \end{aligned} \quad (29)$$

with  $E_{sv,\alpha}^N = \frac{\rho_{\alpha} h_{\alpha} u_{\alpha}^2}{2} + \frac{g \rho_{\alpha} (z_{\alpha+1/2}^2 - z_{\alpha-1/2}^2)}{2}$ .

Adding the preceding relations for  $\alpha = 1, \dots, N$ , we obtain the global balance

$$\frac{\partial}{\partial t} \left( \sum_{\alpha=1}^N E_{sv,\alpha}^N \right) + \frac{\partial}{\partial x} \left( \sum_{\alpha=1}^N u_{\alpha} \left( E_{sv,\alpha}^N + \frac{g}{2} \rho_{\alpha} h_{\alpha} H \right) \right) = 0.$$

**Remark 3.1.** *Neglecting friction and viscosity, the multilayer system (19), (20) approximates the hydrostatic free surface Euler system with varying density that in general is not a hyperbolic system. The hyperbolicity of the multilayer model is still an open question and it is not investigated here. We refer to [5] for a discussion on the hyperbolicity of the multilayer system with constant density. In the work [5] the authors prove the hyperbolic character of the constant density model for the special case of two layers. Let us also remark that the numerical scheme for the multilayer system detailed in the following is able to overcome the difficulty of possible lack of hyperbolicity (Sec. 5).*

### 3.3. Vertical velocity

In Prop. 1 the vertical velocity  $w$  no more appears, but we can derive relations for the discrete layer values of this variable by performing the Galerkin approximation of the continuity equation (1) multiplied by  $z$ . This leads to

$$\frac{\partial}{\partial t} \left( \frac{z_{\alpha+1/2}^2 - z_{\alpha-1/2}^2}{2} \rho_{\alpha} \right) + \frac{\partial}{\partial x} \left( \frac{z_{\alpha+1/2}^2 - z_{\alpha-1/2}^2}{2} \rho_{\alpha} u_{\alpha} \right) = h_{\alpha} \rho_{\alpha} w_{\alpha} + z_{\alpha+1/2} G_{\alpha+1/2} - z_{\alpha-1/2} G_{\alpha-1/2}, \quad (30)$$

where the  $w_\alpha$ ,  $\alpha = 1, \dots, N$ , are the components of the Galerkin approximation of  $w$  on  $\mathbb{P}_{0,H}^{N,t}$ , see (17). Since all the quantities except  $w_\alpha$  appearing in Eq. (30) are already defined by (19), (20), (21), relation (30) allows obtaining the values  $w_\alpha$  by post-processing. Note that we use the relation (30) rather than the divergence free condition for stability purposes and for the reasons mentioned in the Remark 2.1. We refer the reader to [24] for more details.

### 3.4. Multilayer system vs. Navier–Stokes system

Compared to the initial Navier–Stokes system (1)-(5), the multilayer formulation (19)-(21), (29) and (30) shows advantageous features for the conception of a numerical solution method. The main benefits are the following.

- There is no more derivative with respect to the  $z$  direction;
- The water depth  $H$  can be treated as a dynamical variable;
- The geometrical domain is completely defined once the variable  $H$  is known. This point, together with the two features above, means that at the discrete level only a fixed mesh of the domain in the  $x$ -direction is necessary to represent a bidimensional ( $x - z$ ) problem with a moving boundary.
- The system (19)-(21), (29) has the structure of a system of conservation laws with source terms. This enables employing stable and robust numerical techniques extensively developed for the approximation of similar systems of PDEs, in particular for handling efficiently wet/dry fronts and modelling correctly equilibrium states.

We will take advantage of these properties at the discrete level, see Section 5.

## 4. Kinetic interpretation

In this section, we propose a kinetic interpretation for the system (19)-(21) completed with the relations (25), (26) and (27).

The kinetic approach consists in using a description of the microscopic behavior of the system [25]. In this method, fictitious particles are introduced and the equations are considered at the microscopic scale, where no discontinuities occur. The kinetic interpretation of a system allows its transformation into a linear transport equation, to which an upwinding discretization is naturally applicable.

### 4.1. Kinetic interpretation of the multilayer model

The procedure to obtain the kinetic interpretation of the multilayer model with varying density is analogous to the one used in [5], see also [26]. Originally, the kinetic approach was used for conservation laws [25]. Here we extend the kinetic representation to systems with source terms. The kinetic technique allows obtaining an energy equality and a CFL condition at the microscopic level.

For a given layer  $\alpha$ , a distribution function  $M_\alpha(x, t, \xi)$  of fictitious particles with microscopic velocity  $\xi$  is introduced to obtain a linear kinetic equation equivalent to the macroscopic model presented in Prop. 1.

Let us introduce a real function  $\chi$  defined on  $\mathbb{R}$ , compactly supported, and endowed with the following properties

$$\begin{cases} \chi(-w) = \chi(w) \geq 0, \\ \int_{\mathbb{R}} \chi(w) dw = \int_{\mathbb{R}} w^2 \chi(w) dw = 1. \end{cases} \quad (31)$$

Now let us construct a density of particles  $M_\alpha(x, t, \xi)$  defined by a Gibbs equilibrium: the microscopic density of particles present at time  $t$ , in the layer  $\alpha$ , at the abscissa  $x$  and with velocity  $\xi$  given by

$$M_\alpha = \frac{\rho_\alpha h_\alpha(x, t)}{c_\alpha} \chi\left(\frac{\xi - u_\alpha(x, t)}{c_\alpha}\right), \quad (32)$$

with

$$c_\alpha^2 = \frac{p_\alpha}{\rho_\alpha},$$

and  $p_\alpha$  defined by (27).

Likewise, we define  $N_{\alpha+1/2}(x, t, \xi)$  and  $S_{\alpha+1/2}(x, t, \xi)$  by

$$N_{\alpha+1/2}(x, t, \xi) = G_{\alpha+1/2}(x, t) \delta(\xi - u_{\alpha+1/2}(x, t)), \quad (33)$$

$$S_{\alpha+1/2}(x, t, \xi) = p_{\alpha+1/2}(x, t) \frac{\partial z_{\alpha+1/2}}{\partial x} \frac{\partial}{\partial \xi} \delta\left(\xi - \left(u_{\alpha+1/2}(x, t) - \frac{w_{\alpha+1/2}(x, t)}{\frac{\partial z_{\alpha+1/2}}{\partial x}}\right)\right), \quad (34)$$

for  $\alpha = 0, \dots, N$ , and where  $\delta$  denotes the Dirac distribution. Relation (34) will be used to obtain an energy equality.

The quantities  $G_{\alpha+1/2}$ ,  $0 \leq \alpha \leq N$ , represent the mass exchanges between layers  $\alpha$  and  $\alpha + 1$ . They are defined in (25) and satisfy the conditions (24), so  $N_{1/2}$  and  $N_{N+1/2}$  also satisfy

$$N_{1/2}(x, t, \xi) = N_{N+1/2}(x, t, \xi) = 0. \quad (35)$$

For the temperature, we have the equilibria

$$U_\alpha(x, t, \xi) = T_\alpha(x, t) M_\alpha(x, t, \xi), \quad \alpha = 1, \dots, N, \quad (36)$$

$$V_{\alpha+1/2}(x, t, \xi) = T_{\alpha+1/2}(x, t) N_{\alpha+1/2}(x, t, \xi), \quad \alpha = 0, \dots, N. \quad (37)$$

With the previous definitions we write a kinetic representation of the system described in Prop. 1 and we can state the following proposition:

**Proposition 2.** *The functions  $(H, u^N, T^N)$  are strong solutions of the system (19)-(21) if and only if the set of equilibria  $\{M_\alpha(x, t, \xi), U_\alpha(x, t, \xi)\}_{\alpha=1}^N$  is a solution of the kinetic equations*

$$\frac{\partial M_\alpha}{\partial t} + \xi \frac{\partial M_\alpha}{\partial x} - N_{\alpha+1/2} - S_{\alpha+1/2} + N_{\alpha-1/2} + S_{\alpha-1/2} = Q_{M_\alpha}, \quad (38)$$

$$\frac{\partial U_\alpha}{\partial t} + \xi \frac{\partial U_\alpha}{\partial x} - V_{\alpha+1/2} + V_{\alpha-1/2} = Q_{U_\alpha}, \quad (39)$$

for  $\alpha = 1, \dots, N$ , with  $\{N_{\alpha+1/2}(x, t, \xi), S_{\alpha+1/2}(x, t, \xi), V_{\alpha+1/2}(x, t, \xi)\}_{\alpha=0}^N$  satisfying (33)-(37).

The quantities  $Q_{M_\alpha} = Q_{M_\alpha}(x, t, \xi)$  and  $Q_{U_\alpha} = Q_{U_\alpha}(x, t, \xi)$  are ‘‘collision terms’’ equal to zero at the macroscopic level, i.e. they satisfy a.e. for values of  $(x, t)$

$$\int_{\mathbb{R}} Q_{M_\alpha} d\xi = 0, \quad \int_{\mathbb{R}} \xi Q_{M_\alpha} d\xi = 0, \quad \text{and} \quad \int_{\mathbb{R}} Q_{U_\alpha} d\xi = 0. \quad (40)$$

**Proof.** Using the definitions (32), (36) and the properties (31) of the function  $\chi$ , we have

$$\rho_\alpha h_\alpha = \int_{\mathbb{R}} M_\alpha(x, t, \xi) d\xi, \quad \rho_\alpha h_\alpha u_\alpha = \int_{\mathbb{R}} \xi M_\alpha(x, t, \xi) d\xi, \quad (41)$$

$$\rho_\alpha h_\alpha T_\alpha = \int_{\mathbb{R}} U_\alpha(x, t, \xi) d\xi, \quad \rho_\alpha h_\alpha T_\alpha u_\alpha = \int_{\mathbb{R}} \xi U_\alpha(x, t, \xi) d\xi. \quad (42)$$

From the definitions (33), (34) of  $N_{\alpha+1/2}$  and  $S_{\alpha+1/2}$ , we also have

$$\int_{\mathbb{R}} N_{\alpha+1/2}(x, t, \xi) d\xi = G_{\alpha+1/2}, \quad (43)$$

$$\int_{\mathbb{R}} \xi N_{\alpha+1/2}(x, t, \xi) d\xi = u_{\alpha+1/2} G_{\alpha+1/2}, \quad (44)$$

$$\int_{\mathbb{R}} S_{\alpha+1/2}(x, t, \xi) d\xi = 0, \quad (45)$$

$$\int_{\mathbb{R}} \xi S_{\alpha+1/2}(x, t, \xi) d\xi = p_{\alpha+1/2} \frac{\partial z_{\alpha+1/2}}{\partial x}. \quad (46)$$

Then, using (40), (43), (45), the equation (38) integrated in  $\xi$  gives, for each layer  $\alpha$ , the equation (22). Then, with the conditions (35), the sum of the equations (38) gives the continuity equation (19). Likewise the equations (38) integrated in  $\xi$  against  $\xi$  give the momentum equations (20). Finally a simple integration in  $\xi$  of the equations (39), again using (40), gives the tracer equations (21).  $\square$

#### 4.2. Vertical velocity kinetic equation

In order to capture the macroscopic vertical velocities  $w_\alpha$  at the continuous level, the kinetic interpretation has to take into account the microscopic vertical velocity  $\gamma$  of the particles. For a given layer  $\alpha \in [1, \dots, N]$ , we construct the new densities of particles  $R_\alpha(x, t, \xi, \gamma)$  defined by the Gibbs equilibria: the microscopic density of particles present at time  $t$ , position  $x$  and with microscopic horizontal velocity  $\xi$  and microscopic vertical velocity  $\gamma$  given by

$$R_\alpha(x, t, \xi, \gamma) = \rho_\alpha \frac{z_{\alpha+1/2}^2 - z_{\alpha-1/2}^2}{2} \delta(\xi - u_\alpha) \delta(\gamma - w_\alpha), \quad (47)$$

and satisfying the kinetic equations

$$\frac{\partial R_\alpha}{\partial t} + \xi \frac{\partial R_\alpha}{\partial x} - \delta(\gamma - w_\alpha) (\gamma M_\alpha - z_{\alpha+1/2} N_{\alpha+1/2} + z_{\alpha-1/2} N_{\alpha-1/2}) = Q_{R_\alpha}, \quad (48)$$

where  $Q_{R_\alpha} = Q_{R_\alpha}(x, t, \xi, \gamma)$  is a collision term satisfying

$$\int_{\mathbb{R}^2} Q_{R_\alpha} d\xi d\gamma = 0. \quad (49)$$

Using (49) a simple integration in  $\xi$  and  $\gamma$  of Eq. (48) gives (30).

#### 4.3. Kinetic interpretation of energy equation

In order to recover, for smooth solutions, the energy balances (29), we also introduce for  $\alpha = 1, \dots, N$  the densities  $\widetilde{M}_\alpha(x, t, \xi)$  defined by

$$\widetilde{M}_\alpha = \frac{h_\alpha(x, t) p_\alpha(x, t)}{2} \delta(\xi - u_\alpha(x, t)),$$

and we have the following proposition

**Proposition 3.** *The solutions of (38), (39) and (48) are entropy solutions if additionally*

$$\frac{\partial \widetilde{M}_\alpha}{\partial t} + \xi \frac{\partial \widetilde{M}_\alpha}{\partial x} = \widetilde{Q}_\alpha(x, t, \xi), \quad \alpha = 1, \dots, N, \quad (50)$$

with for smooth solutions

$$\sum_{\alpha=1}^N \left( \int_{\mathbb{R}} \left( \frac{\xi^2}{2} Q_{M_\alpha} - \widetilde{Q}_\alpha \right) d\xi + g \int_{\mathbb{R}^2} Q_{R_\alpha} d\xi d\gamma \right) = 0. \quad (51)$$

**Proof:** The proof is obtained by simple integration in  $\xi, \gamma$  of the set of equations (38), (39) and (50) using (40), (49) and (51). Indeed from the definitions (32), (33) and (47) we have

$$\begin{aligned}
\rho_\alpha h_\alpha u_\alpha^3 + \frac{h_\alpha}{2} p_\alpha u_\alpha &= \int_{\mathbb{R}} \xi^3 M_\alpha(x, t, \xi) d\xi, \\
\rho_\alpha h_\alpha w_\alpha &= \int_{\mathbb{R}^2} \gamma \delta(\gamma - w_\alpha) M_\alpha(x, t, \xi) d\xi d\gamma, \\
h_\alpha p_\alpha u_\alpha &= \int_{\mathbb{R}} \xi \widetilde{M}_\alpha(x, t, \xi) d\xi, \quad u_{\alpha+1/2}^2 = \int_{\mathbb{R}} \xi^2 N_{\alpha+1/2}(x, t, \xi) d\xi, \\
G_{\alpha+1/2} &= \int_{\mathbb{R}^2} \delta(\gamma - w_\alpha) N_{\alpha+1/2}(x, t, \xi) d\xi d\gamma, \\
\rho_\alpha \frac{z_{\alpha+1/2}^2 - z_{\alpha-1/2}^2}{2} &= \int_{\mathbb{R}^2} R_\alpha(x, t, \xi, \gamma) d\xi d\gamma, \\
\rho_\alpha \frac{z_{\alpha+1/2}^2 - z_{\alpha-1/2}^2}{2} u_\alpha &= \int_{\mathbb{R}^2} \xi R_\alpha(x, t, \xi, \gamma) d\xi d\gamma, \\
2p_{\alpha+1/2} \frac{\partial z_{\alpha+1/2}}{\partial x} u_{\alpha+1/2} &= \int_{\mathbb{R}} \xi^2 S_{\alpha+1/2}(x, t, \xi) d\xi. \quad \square
\end{aligned}$$

## 5. Numerical scheme

We have shown in Section 2 that a Galerkin vertical discretization of the Navier–Stokes equations leads to the multilayer model system presented in Section 3. Now, we propose a finite volume numerical scheme for the approximation of this model based on the kinetic interpretation of the system equations illustrated in Section 4.

The choice of a kinetic scheme is motivated by several arguments. First, the kinetic interpretation is a suitable starting point for building a stable numerical scheme. We will prove in Sec. 5.8 that the proposed kinetic scheme preserves positivity of the water depth and ensures a discrete local maximum principle for the tracer concentration (temperature, salinity...). Second, the construction of the kinetic scheme does not need the computation of the system eigenvalues. This point is very important here since these eigenvalues are not available in explicit analytical form, and they are hardly accessible even numerically. Furthermore, as previously mentioned, hyperbolicity of the multilayer model may not hold, and the kinetic scheme allows overcoming this difficulty.

The multilayer system obtained in Prop. 1 has the form

$$\frac{\partial X}{\partial t} + \frac{\partial F(X)}{\partial x} = S_e(X, \partial_t X, \partial_x X) + S_p(X) + S_{v,f}(X), \quad (52)$$

with  $X = \left( \sum_{\alpha=1}^N \rho_\alpha h_\alpha, q_1, \dots, q_N, k_1, \dots, k_N \right)^T$  and  $q_\alpha = l_\alpha H$ ,  $q_\alpha = \rho_\alpha l_\alpha H u_\alpha$ ,  $k_\alpha = \rho_\alpha l_\alpha H T_\alpha$ . We denote with  $F(X)$  the flux of the conservative part, and with  $S_e(X, \partial_t X, \partial_x X)$ ,  $S_p(X)$  and  $S_{v,f}(X)$  the source terms, representing respectively the mass transfer, the interface pressure, and the viscous and friction effects.

We introduce a  $(2N+1) \times 2N$  matrix  $\mathcal{K}(\xi)$  defined by  $\mathcal{K}_{1,j} = 1$ ,  $\mathcal{K}_{1,j+N} = 0$  for  $j = 1, \dots, N$ ,  $\mathcal{K}_{i+1,j} = \delta_{i,j}$ ,  $\mathcal{K}_{i+N+1,j+N} = \delta_{i,j}$  for  $i, j = 1, \dots, N$  with  $\delta_{i,j}$  the Kronecker symbol. Then, using Prop. 2, we can write

$$X = \int_{\xi} \mathcal{K}(\xi) \begin{pmatrix} M(\xi) \\ U(\xi) \end{pmatrix} d\xi, \quad F(X) = \int_{\xi} \xi \mathcal{K}(\xi) \begin{pmatrix} M(\xi) \\ U(\xi) \end{pmatrix} d\xi, \quad (53)$$

$$S_e(X) = \int_{\xi} \mathcal{K}(\xi) \begin{pmatrix} N(\xi) \\ V(\xi) \end{pmatrix} d\xi, \quad S_p(X) = \int_{\xi} \mathcal{K}(\xi) \begin{pmatrix} P(\xi) \\ 0 \end{pmatrix} d\xi, \quad (54)$$

with  $M(\xi) = (M_1(\xi), \dots, M_N(\xi))^T$ ,  $U(\xi) = (U_1(\xi), \dots, U_N(\xi))^T$  and

$$P(\xi) = \begin{pmatrix} S_{3/2}(\xi) - S_{1/2}(\xi) \\ \vdots \\ S_{N+1/2}(\xi) - S_{N-1/2}(\xi) \end{pmatrix}, \quad \text{and} \quad W(\xi) = \begin{pmatrix} W_{3/2}(\xi) - W_{1/2}(\xi) \\ \vdots \\ W_{N+1/2}(\xi) - W_{N-1/2}(\xi) \end{pmatrix}, \quad \text{for } W = N, V,$$

We refer to [5] for the computation of  $S_{v,f}(X)$ .

To approximate the solution of (52) we use a finite volume framework. We assume that the computational domain is divided into  $I$  nodes  $x_i$ . We denote  $C_i$  the cell of length  $\Delta x_i = x_{i+1/2} - x_{i-1/2}$  with  $x_{i+1/2} = (x_i + x_{i+1})/2$ . For the time discretization, we denote  $t^n = \sum_{k < n} \Delta t^k$ , where the time steps  $\Delta t^k$  will be determined through a CFL condition. We denote  $X_i^n = \left( \sum_{\alpha=1}^N \rho_{\alpha,i}^n l_{\alpha} H_i^n, q_{1,i}^n, \dots, q_{N,i}^n, k_{1,i}^n, \dots, k_{N,i}^n \right)^T$  the approximate solution at time  $t^n$  on the cell  $C_i$  with  $q_{\alpha,i}^n = \rho_{\alpha,i}^n l_{\alpha} H_i^n u_{\alpha,i}^n$ ,  $k_{\alpha,i}^n = \rho_{\alpha,i}^n l_{\alpha} H_i^n T_{\alpha,i}^n$  and  $\rho_{\alpha,i}^n = \rho(T_{\alpha,i}^n)$ . Note that to deduce the primitive variables  $H_i^n, u_{1,i}^n, \dots, u_{N,i}^n, T_{1,i}^n, \dots, T_{N,i}^n$  from  $X_i^n$  a non-linear problem has to be solved (see Sec.5.7).

### 5.1. Time discretization

For the time discretization, we apply a time splitting technique to the equations (52) and we write

$$\frac{\tilde{X}^{n+1} - X^n}{\Delta t^n} + \frac{\partial F(X^n)}{\partial x} = S_e(X^n, \tilde{X}^{n+1}) + S_p(X^n), \quad (55)$$

$$\frac{X^{n+1} - \tilde{X}^{n+1}}{\Delta t^n} - S_{v,f}(X^n, X^{n+1}) = 0. \quad (56)$$

We first solve the conservative part of (55) by the proposed explicit kinetic scheme (Sec. 5.2 and 5.3). The mass exchange terms are also computed via the kinetic interpretation (Sec. 5.4). The first step also includes the pressure source terms at the interfaces in order to preserve relevant equilibria [13]. Concerning the viscous and friction terms  $S_{v,f}$  in (56), they have been omitted in the derivation of the multilayer system (52). Since their expression does not depend on the fluid density  $\rho$ , their vertical discretization and their numerical treatment do not differ from earlier works of the authors [5]. Since these terms are dissipative, they are treated via a semi-implicit scheme for stability reasons.

### 5.2. Discrete kinetic equations

We here illustrate the discrete kinetic equations corresponding to the first step (55).

Starting from a piecewise constant approximation of the initial data, the general form of a finite volume discretization of system (55) is

$$\tilde{X}_i^{n+1} - X_i^n + \sigma_i^n \left[ F_{i+1/2}^n - F_{i-1/2}^n \right] = \Delta t^n \mathcal{S}_{e,i}^{n+1/2} + \sigma_i^n \mathcal{S}_{p,i}^n, \quad (57)$$

where  $\sigma_i^n = \Delta t^n / \Delta x_i$  is the ratio between the time step and the mesh width, and the numerical flux  $F_{i+1/2}^n$  is an approximation of the exact flux estimated at the point  $x_{i+1/2}$ .

The pressure terms at the layer interfaces  $\mathcal{S}_{p,i}^n$  are not deduced from the kinetic interpretation (see [12]) but computed via hydrostatic reconstruction, see Sec. 5.5. As in [27, 26] the kinetic interpretation (38)-(39) is used to specify the expression of the fluxes  $F_{i+1/2}^n$  in (57). Assuming that the primitive variables  $H_i^n, u_{1,i}^n, \dots, u_{N,i}^n, T_{1,i}^n, \dots, T_{N,i}^n$  are known, by analogy with (32) we first define the discrete densities of particles  $M_{\alpha,i}^n$  by

$$M_{\alpha,i}^n(\xi) = \rho_{\alpha,i}^n l_{\alpha} \frac{H_i^n}{c_{\alpha,i}^n} \chi \left( \frac{\xi - u_{\alpha,i}^n}{c_{\alpha,i}^n} \right), \quad \text{with } c_{\alpha,i}^n = \sqrt{\frac{p_{\alpha,i}^n}{\rho_{\alpha,i}^n}},$$

and following (27)

$$p_{\alpha,i}^n = g \left( \frac{\rho_{\alpha,i}^n l_{\alpha} H_i^n}{2} + \sum_{j=\alpha+1}^N \rho_{j,i}^n l_j H_i^n \right).$$

Then the equation (38) is discretised for each  $\alpha$  by applying a simple upwind scheme

$$\begin{aligned} f_{\alpha,i}^{n+1}(\xi) &= M_{\alpha,i}^n(\xi) - \xi \sigma_i^n \left( M_{\alpha,i+1/2}^n(\xi) - M_{\alpha,i-1/2}^n(\xi) \right) + \\ &\Delta t^n \left( N_{\alpha+1/2,i}^{n+1/2}(\xi) - N_{\alpha-1/2,i}^{n+1/2}(\xi) \right) + \Delta t^n \left( S_{\alpha+1/2,i}^n(\xi) - S_{\alpha-1/2,i}^n(\xi) \right), \end{aligned} \quad (58)$$

where

$$M_{\alpha,i+1/2}^n = \begin{cases} M_{\alpha,i}^n & \text{if } \xi \geq 0, \\ M_{\alpha,i+1}^n & \text{if } \xi < 0. \end{cases} \quad (59)$$

The terms  $N_{\alpha+1/2,i}^{n+1/2}$  (resp.  $S_{\alpha+1/2,i}^n$ ) will be defined in Sec. 5.4 (resp. 5.5).

The quantity  $f_{\alpha,i}^{n+1}$  is not an equilibrium, nonetheless by analogy with the proof of Prop. 2, we set

$$\rho_{\alpha,i}^{n+1} l_{\alpha} H_i^{n+1} = \int_{\mathbb{R}} f_{\alpha,i}^{n+1}(\xi) d\xi, \quad (60)$$

and

$$\rho_{\alpha,i}^{n+1} l_{\alpha} H_i^{n+1} u_{\alpha}^{n+1} = \int_{\mathbb{R}} \xi f_{\alpha,i}^{n+1}(\xi) d\xi, \quad (61)$$

thus recovering the macroscopic quantities at time  $t^{n+1}$ .

An upwind scheme similar to (58) is applied to Eq. (39), giving, with obvious notations,

$$\begin{aligned} g_{\alpha,i}^{n+1}(\xi) &= U_{\alpha,i}^n(\xi) - \xi \sigma_i^n \left( U_{\alpha,i+1/2}^n(\xi) - U_{\alpha,i-1/2}^n(\xi) \right) + \\ &\Delta t^n \left( V_{\alpha+1/2,i}^{n+1/2}(\xi) - V_{\alpha-1/2,i}^{n+1/2}(\xi) \right), \end{aligned} \quad (62)$$

and allowing recovering the macroscopic quantities

$$\rho_{\alpha,i}^{n+1} l_{\alpha} H_i^{n+1} T_{\alpha,i}^{n+1} = \int_{\mathbb{R}} g_{\alpha,i}^{n+1}(\xi) d\xi. \quad (63)$$

The equations (60), (61), (63) are summarized here in compact form:

$$\tilde{X}_i^{n+1} = \int_{\xi} \mathcal{K}(\xi) \begin{pmatrix} f_i^{n+1}(\xi) \\ g_i^{n+1}(\xi) \end{pmatrix} d\xi, \quad (64)$$

with  $f_i^n(\xi) = (f_{1,i}^n(\xi), \dots, f_{N,i}^n(\xi))^T$ ,  $g_i^n(\xi) = (g_{1,i}^n(\xi), \dots, g_{N,i}^n(\xi))^T$ .

Note that in (58) the collisions terms  $Q_{M_{\alpha}}$ , which relax  $f$  to a Gibbs equilibrium  $M$ , are not taken into account, they are added by introducing a discontinuity at time  $t^{n+1}$  on  $M_{\alpha,i}$ . Assuming that the primitive variables are computed at time  $t^{n+1}$ , we set

$$M_{\alpha,i}^{n+1}(\xi) = \rho_{\alpha,i}^{n+1} l_{\alpha} \frac{H_i^{n+1}}{c_{\alpha,i}^{n+1}} \chi \left( \frac{\xi - u_{\alpha,i}^{n+1}}{c_{\alpha,i}^{n+1}} \right).$$

We apply the same remark to  $U_{\alpha,i}$ . From the previous definitions  $M_{\alpha,i}$  and  $U_{\alpha,i}$  are discontinuous at time

$t^{n+1}$  in the sense that  $M_{\alpha,i}^{n+1} \neq f_{\alpha,i}^{n+1}$  and  $U_{\alpha,i}^{n+1} \neq g_{\alpha,i}^{n+1}$ , but at the macroscopic level we have

$$\int_{\mathbb{R}} M_{\alpha,i}^{n+1} d\xi = \int_{\mathbb{R}} f_{\alpha,i}^{n+1} d\xi, \quad \int_{\mathbb{R}} U_{\alpha,i}^{n+1} d\xi = \int_{\mathbb{R}} g_{\alpha,i}^{n+1} d\xi.$$

### 5.3. Numerical fluxes of the conservative part

In this section we give some details for the computation of the fluxes introduced in the discrete equation (57), and defined by (64) using (58) and (62). To take into account (59), we denote

$$F_{i+1/2}^n = F(X_i^n, X_{i+1}^n) = F^+(X_i^n) + F^-(X_{i+1}^n), \quad (65)$$

and following (53), we define

$$F^-(X_i^n) = \int_{\xi \in \mathbb{R}^-} \xi \mathcal{K}(\xi) \begin{pmatrix} M_i^n(\xi) \\ U_i^n(\xi) \end{pmatrix} d\xi, \quad F^+(X_i^n) = \int_{\xi \in \mathbb{R}^+} \xi \mathcal{K}(\xi) \begin{pmatrix} M_i^n(\xi) \\ U_i^n(\xi) \end{pmatrix} d\xi \quad (66)$$

with  $M_i^n(\xi) = (M_{1,i}^n(\xi), \dots, M_{N,i}^n(\xi))^T$ ,  $U_i^n(\xi) = (U_{1,i}^n(\xi), \dots, U_{N,i}^n(\xi))^T$ .

More precisely the expression of  $F^+(X_i)$  can be written

$$F^+(X_i) = (F_H^+(X_i), F_{q_1}^+(X_i), \dots, F_{q_N}^+(X_i), F_{k_1}^+(X_i), \dots, F_{k_N}^+(X_i))^T, \quad (67)$$

with, using (58) and (64),

$$F_H^+(X_i) = \sum_{\alpha=1}^N F_{h_\alpha}^+(X_i) = \sum_{\alpha=1}^N \rho_{\alpha,i} l_\alpha H_i \int_{w \geq -\frac{u_{\alpha,i}}{c_i}} (u_{\alpha,i} + w c_{\alpha,i}) \chi(w) dw, \quad (68)$$

$$F_{q_\alpha}^+(X_i) = \rho_{\alpha,i} l_\alpha H_i \int_{w \geq -\frac{u_{\alpha,i}}{c_i}} (u_{\alpha,i} + w c_{\alpha,i})^2 \chi(w) dw, \quad (69)$$

$$F_{k_\alpha}^+(X_i) = T_{\alpha,i} F_{h_\alpha}^+(X_i). \quad (70)$$

We denote also

$$\mathcal{F}_{h_\alpha,i} = F_{h_\alpha,i+1/2} - F_{h_\alpha,i-1/2} = F_{h_\alpha}^+(X_i) + F_{h_\alpha}^-(X_{i+1}) - (F_{h_\alpha}^+(X_{i-1}) + F_{h_\alpha}^-(X_i)). \quad (71)$$

One attractive feature of the kinetic method is that it provides a very simple and natural way to construct a numerical flux through the kinetic interpretation. Indeed, choosing

$$\chi(w) = \frac{1}{2\sqrt{3}} \mathbf{1}_{|w| \leq \sqrt{3}}(w),$$

the integration in (67) can be done analytically.

### 5.4. Discrete mass exchange terms

Let us now define the mass exchange term  $\mathcal{S}_{e,i}^{n+1/2}$  in the equation (57), or more precisely the terms  $N_{\alpha+1/2,i}^{n+1/2}$  in Eq. (58). From the conditions (35) we prescribe

$$N_{1/2,i}^{n+1/2}(\xi) = N_{N+1/2,i}^{n+1/2}(\xi) = 0, \quad (72)$$

and using the discrete analogous of Eq. (45) (see Eq. (79) in Sec. 5.5) the sum for all  $\alpha$  of Eq. (60) defines explicitly  $\sum_{\alpha=1}^N \rho_{\alpha,i}^{n+1} l_\alpha H_i^{n+1}$ .

Likewise, by partial summation of (58), we have

$$\Delta t^n N_{\alpha+1/2,i}^{n+1/2}(\xi) + \Delta t^n S_{\alpha+1/2,i}^{n+1/2}(\xi) = \sum_{j=1}^{\alpha} \left( f_{j,i}^{n+1}(\xi) - M_{j,i}^n(\xi) + \xi \sigma_i^n \left( M_{j,i+1/2}^n(\xi) - M_{j,i-1/2}^n(\xi) \right) \right), \quad (73)$$

for  $\alpha = 1, \dots, N-1$ .

By analogy with (43), we define

$$G_{\alpha+1/2,i}^{n+1/2} = \int_{\mathbb{R}} N_{\alpha+1/2,i}^{n+1/2}(\xi) d\xi, \quad \alpha = 0, \dots, N, \quad (74)$$

thus, using (60) and (79), we can write

$$\Delta t^n G_{\alpha+1/2,i}^{n+1/2} = \sum_{j=1}^{\alpha} \left[ l_j (\rho_{j,i}^{n+1} H_i^{n+1} - \rho_{j,i}^n H_i^n) + \sigma_i^n (F_{hj,i+1/2}^n - F_{hj,i-1/2}^n) \right], \quad (75)$$

for  $\alpha = 1, \dots, N$ . We remark that this expression is consistent with the free surface condition in (72). Let us note that the definition (75) depends on  $\rho_{\alpha,i}^{n+1} H_i^{n+1}$ , which reflects the dependence of  $G_{\alpha+1/2}$  on the time derivatives  $\partial_t(\rho_j h_j)$ ,  $j = 1, \dots, \alpha$  (see eq. (25)). These values  $\rho_{\alpha,i}^{n+1} H_i^{n+1}$  are unknown at this stage since only the global quantity  $\sum_{\alpha=1}^N \rho_{\alpha,i}^{n+1} l_{\alpha} H_i^{n+1}$  can be explicitly computed. This is the reason why we choose to denote the discrete mass exchange terms with time level  $(n+1/2)$ ,  $G_{\alpha+1/2,i}^{n+1/2}$ , and similarly we use the notation  $N_{\alpha+1/2,i}^{n+1/2}$ ,  $V_{\alpha+1/2,i}^{n+1/2}$  and  $S_{e,i}^{n+1/2}$ . As a consequence we will have to solve a nonlinear system to compute the quantities of interest at time  $t^{n+1}$ , see Sec. 5.7.

We define

$$N_{\alpha+1/2,i}^{n+1/2}(\xi) = G_{\alpha+1/2,i}^{n+1/2} \delta(\xi - u_{\alpha+1/2,i}^n), \quad V_{\alpha+1/2,i}^{n+1/2}(\xi) = T_{\alpha+1/2,i}^n N_{\alpha+1/2,i}^{n+1/2}(\xi) \quad (76)$$

with, according to (28),

$$v_{\alpha+1/2,i}^n = \begin{cases} v_{\alpha+1,i}^n & \text{if } G_{\alpha+1/2,i}^{n+1/2} \geq 0, \\ v_{\alpha,i}^n & \text{if } G_{\alpha+1/2,i}^{n+1/2} < 0, \end{cases} \quad (77)$$

for  $v = u, T$ . Let us stress also here the dependence of the interface values in the above definition on the quantities  $G_{\alpha+1/2,i}^{n+1/2}$  not explicitly available at time  $t^{n+1}$ . The way to overcome this difficulty will be explained when we will illustrate the numerical solution technique for the nonlinear problem in Sec. 5.7. Nevertheless we can now consider that the exchange term  $S_{e,i}^{n+1/2}$  in (57) is completely defined.

### 5.5. Numerical treatment of pressure source terms

We focus now on the source term  $S_{p,i}^n$  in (57) associated to the interface pressure, namely the discretization of  $S_{\alpha+1/2}(x, t, \xi)$  defined by (27), (34). The terms  $S_{p,i}^n$  are defined in such a way to preserve steady states conditions of a lake at rest. The numerical treatment that we propose here for these source pressure terms is different from what it is usually done in the hydrostatic reconstruction method [13], and from what has been proposed by the authors in [5]. Nevertheless in the case of a single layer with a constant density, and for the first order scheme, the source term discretization that we present here is similar to the formulation given in [13].

From the kinetic interpretation (38), and using the definition (34), we point out that we can write

$$S_{p,i}^n = \int_{\xi} \mathcal{K}(\xi) \begin{pmatrix} P_i^n(\xi) \\ 0 \end{pmatrix} d\xi, \quad (78)$$

with

$$P_{\alpha,i}^n(\xi) = S_{\alpha+1/2,i}^n(\xi) - S_{\alpha-1/2,i}^n(\xi).$$

We have the discrete analogous of Eq. (45):

$$\int_{\mathbb{R}} S_{\alpha+1/2,i}^n(\xi) d\xi = 0. \quad (79)$$

The term

$$\int_{\mathbb{R}} \xi S_{\alpha+1/2,i}^n(\xi) d\xi,$$

which is an approximation of

$$\int_{x_{i-1/2}}^{x_{i+1/2}} \frac{\partial z_{\alpha+1/2}(x, t^n)}{\partial x} p_{\alpha+1/2}(x, t^n) dx,$$

is defined hereafter.

As for the classical hydrostatic reconstruction [13], we introduce

$$z_{b,i+1/2} = \max\{z_{b,i}, z_{b,i+1}\}, \quad (80)$$

$$H_{i+1/2-}^n = H_i^n + z_{b,i} - z_{b,i+1/2}, \quad (81)$$

$$H_{i+1/2+}^n = H_{i+1}^n + z_{b,i+1} - z_{b,i+1/2}, \quad (82)$$

$$h_{\alpha,i+1/2\pm}^n = l_{\alpha} H_{i+1/2\pm}^n. \quad (83)$$

Then, following (16), we set

$$z_{\alpha+1/2,i}^n = z_{b,i} + \sum_{j=1}^{\alpha} h_{\alpha,i}^n, \quad z_{\alpha+1/2,i+1/2-}^n = z_{b,i+1/2} + \sum_{j=1}^{\alpha} h_{\alpha,i+1/2-}^n. \quad (84)$$

We also define

$$p_{\alpha+1/2,i+1/4}^n = \frac{p_{\alpha+1/2,i+1/2-}^n + p_{\alpha+1/2,i}^n}{2}, \quad (85)$$

with

$$p_{\alpha+1/2,i}^n = g \sum_{j=\alpha+1}^N \rho_{j,i}^n h_{j,i}^n, \quad p_{\alpha+1/2,i+1/2-}^n = g \sum_{j=\alpha+1}^N \rho_{j,i}^n h_{j,i+1/2-}^n. \quad (86)$$

Then the idea of the numerical treatment of the pressure source term relies on rewriting it under the form

$$\frac{\partial z_{\alpha+1/2}(x, t)}{\partial x} p_{\alpha+1/2}(x, t) = \frac{\partial}{\partial x} \int_{x_0}^x \frac{\partial z_{\alpha+1/2}(\tilde{x}, t)}{\partial \tilde{x}} p_{\alpha+1/2}(\tilde{x}, t) d\tilde{x}.$$

This leads at the discrete level to the formula

$$\begin{aligned} & \int_{x_{i-1/2}}^{x_{i+1/2}} \frac{\partial z_{\alpha+1/2}(x, t^n)}{\partial x} p_{\alpha+1/2}(x, t^n) dx \\ &= \int_{x_i}^{x_{i+1/2}} \frac{\partial z_{\alpha+1/2}(x, t^n)}{\partial x} p_{\alpha+1/2}(x, t^n) dx - \int_{x_i}^{x_{i-1/2}} \frac{\partial z_{\alpha+1/2}(x, t)}{\partial \tilde{x}} p_{\alpha+1/2}(x, t^n) d\tilde{x}, \end{aligned}$$

where the cell-averaged source term is locally represented as a discrete gradient corresponding to a source distributed to the cell interfaces. Then we write

$$\int_{\mathbb{R}} \xi S_{\alpha+1/2,i}^n(\xi) d\xi = S_{\alpha+1/2,i+1/2-}^n - S_{\alpha+1/2,i-1/2+}^n, \quad \alpha = 1, \dots, N, \quad (87)$$

with the definition

$$S_{\alpha+1/2,i+1/2-}^n = p_{\alpha+1/2,i+1/4}^n \left( z_{\alpha+1/2,i+1/2-}^n - z_{\alpha+1/2,i}^n \right). \quad (88)$$

Notice that Eq. (88) is a classical relation/definition allowing to obtain an approximate quadrature formula for the right hand side of (87), whereas Eqs. (80)-(83) correspond to an upwind discretization of the bottom topography using the hydrostatic reconstruction strategy. We also notice that the flux (65) is no more computed using the cell centered values  $h_{\alpha,i}^n$  and  $h_{\alpha,i+1}^n$  but the reconstructed interface values  $h_{\alpha,i+1/2-}^n$  and  $h_{\alpha,i+1/2+}^n$ , i.e.

$$F_{i+1/2}^n = F^+(X_{i+1/2-}^n) + F^-(X_{i+1/2+}^n).$$

One of the major concern for the discretization of the pressure source terms  $\mathcal{S}_{p,i}(X^n)$  is the preservation of relevant equilibria. At the continuous level, the static equilibrium of the lake at rest is given by

$$u(x, z) = 0, \quad \int_z^\eta \rho(x, \tilde{z}) d\tilde{z} = Cst(z), \quad \forall x, z,$$

which implies

$$u = 0, \quad \eta = Cst, \quad \text{and} \quad T = T(z). \quad (89)$$

We first consider the case of constant density, i.e.  $T(x, z, t) = T_0$ , and we have the following proposition.

**Proposition 4.** *If the density is constant, the discretization of the source terms given by (78) preserves the steady state of a “lake at rest” given by (89).*

**Proof.** *Assuming steady state conditions of a lake at rest, we have  $H_i^n + z_{b,i} = H_{i+1}^n + z_{b,i+1}$  and  $u_i^n = 0 \forall i$ . By construction we have  $H_{i+1/2-}^n = H_{i+1/2+}^n$  and  $S_{e,i}^{n+1/2} = 0$  for  $\alpha = 1, \dots, N$ ,  $i \in I$ . Thus  $X_{i+1/2-}^n = X_{i+1/2+}^n$ , and we obtain  $\mathcal{F}_{h_{\alpha,i}} = 0, \forall \alpha, \forall i$ . A simple calculation shows that the expression of the source terms (78) coupled with the flux computed with the kinetic scheme gives  $F_{i+1/2}^n - F_{i-1/2}^n = S_{p,i+1/2-}^n - S_{p,i-1/2+}^n$  with  $S_{p,i+1/2-}^n = (S_{3/2,i+1/2-}^n - S_{1/2,i+1/2-}^n, \dots, S_{N+1/2,i+1/2-}^n - S_{N-1/2,i+1/2-}^n)^T$ , which completes the proof.  $\square$*

### 5.6. Static equilibrium and variable density

When the fluid density varies, the preservation of equilibrium states at rest is more problematic. In the case of flow in static equilibrium over a flat bottom all the interfaces are horizontal, thus at the continuous and discrete level we have

$$\frac{\partial z_{\alpha+1/2}}{\partial x} = 0, \quad \alpha = 1, \dots, N.$$

It follows that  $S_p = 0$  and the equilibrium is obviously preserved.

In the situation of non flat bottom, equilibrium at rest is more difficult to characterize since this corresponds to

$$\frac{\partial h_{\alpha} p_{\alpha}}{\partial x} = \frac{\partial z_{\alpha+1/2}}{\partial x} p_{\alpha+1/2} - \frac{\partial z_{\alpha-1/2}}{\partial x} p_{\alpha-1/2}$$

with possibly an inhomogeneous distribution of the tracer  $T$ .

Instead of proving that our scheme preserves such equilibria, we will show numerically in Sec. 6.1 that starting from a given initial condition, and with no forcing terms and energy supply, the system evolves to a static equilibrium state satisfying

$$\eta_i = Cst, \quad u_{\alpha,i} = 0, \quad \text{and} \quad T(x_i, \{z_{\alpha}\}) = Cst_{\alpha}, \quad \alpha = 1, \dots, N, \quad i \in I,$$

that is the discrete equivalent of the continuous equilibrium (89).

### 5.7. Nonlinear coupling

In Secs. 5.2-5.5 we have described how to compute through the kinetic scheme and an extended hydrostatic reconstruction technique the quantities

$$\sum_{\alpha=1}^N \rho_{\alpha,i}^{n+1} l_{\alpha} H_i^{n+1}, \quad \rho_{\alpha,i}^{n+1} l_{\alpha} H_i^{n+1} u_{\alpha,i}^{n+1} \quad \text{and} \quad \rho_{\alpha,i}^{n+1} l_{\alpha} H_i^{n+1} T_{\alpha,i}^{n+1}. \quad (90)$$

From (60) and (72), we have that the first term is computed explicitly. It is not the case for the third term, since, as anticipated before, the evaluation of the interface flux  $G_{\alpha+1/2,i}^{n+1/2}$  (75) involves quantities computed at time  $t^{n+1}$ . Moreover, the density  $\rho_{\alpha,i}$  is in general a nonlinear function of the tracer (temperature)  $T_{\alpha,i}$ . It follows that a  $(N+1)$  nonlinear problem has to be solved to completely define  $H_i^{n+1}$  and  $T_{\alpha,i}^{n+1}$ . This nonlinear problem reads

$$\begin{aligned} \sum_{\alpha=1}^N \rho_{\alpha,i}^{n+1} l_{\alpha} H_i^{n+1} &= \sum_{\alpha=1}^N \rho_{\alpha,i}^n l_{\alpha} H_i^n + \frac{\Delta t^n}{\Delta x} (F_H^+(X_{i-1}^n) + F_H^-(X_i^n) - F_H^+(X_i^n) - F_H^-(X_{i+1}^n)), \\ \rho_{\alpha,i}^{n+1} l_{\alpha} H_i^{n+1} T_{\alpha,i}^{n+1} &= \rho_{\alpha,i}^n l_{\alpha} H_i^n T_{\alpha,i}^n + \frac{\Delta t^n}{\Delta x} (F_{k_{\alpha}}^+(X_{i-1}^n) + F_{k_{\alpha}}^-(X_i^n) - F_{k_{\alpha}}^+(X_i^n) - F_{k_{\alpha}}^-(X_{i+1}^n)) \\ &\quad + \Delta t (T_{\alpha+1/2,i}^{k,n} G_{\alpha+1/2,i}^{n+1/2} - T_{\alpha-1/2,i}^{k,n} G_{\alpha-1/2,i}^{n+1/2}), \quad \alpha = 1, \dots, N, \end{aligned} \quad (91)$$

where the fluxes  $F^{\pm}$  and  $G$  can be evaluated through the formulas (71) and (75), and the interface values  $T_{\alpha+1/2,i}$  are given by (77). The system above can be written under the form

$$\mathcal{R}(H_i^{n+1}, T_{1,i}^{n+1}, \dots, T_{N,i}^{n+1}) = C_i^n, \quad (92)$$

where the term  $C_i^n$  contains all the data, i.e. the quantities that are evaluated at time  $t^n$ , and the function  $\mathcal{R}$  from  $\mathbb{R}^{N+1}$  to  $\mathbb{R}^{N+1}$  is given by

$$\mathcal{R}(x, y_1, \dots, y_n) = \left( \begin{array}{c} x \sum_{\alpha=1}^N l_{\alpha} \rho(y_{\alpha}) \\ x l_{\alpha} y_{\alpha} \rho(y_{\alpha}) - T_{\alpha+1/2,i}^{k,n} x \sum_{j=1}^{\alpha} l_j \rho(y_j) + T_{\alpha-1/2,i}^{k,n} x \sum_{j=1}^{\alpha-1} l_j \rho(y_j) \end{array} \right).$$

The nonlinear system (92) is solved by using an iterative procedure that defines a sequence of quantities  $(H_i^{k,n}, T_{\alpha,i}^{k,n})$ , where the superscript  $k$  is the iteration counter. Let us note that in the definition of the function  $\mathcal{R}$  the interface value of the tracer  $T_{\alpha+1/2,i}^{k,n}$  is explicitly related to the actual iteration. Indeed formula (77), which was said to be non explicit since the quantity  $G_{\alpha+1/2,i}^{n+1/2}$  is implicitly defined, is replaced in the iterative process by the explicit formula

$$T_{\alpha+1/2,i}^{k,n} = \begin{cases} T_{\alpha+1,i}^n & \text{if } G_{\alpha+1/2,i}^{k-1,n} \geq 0, \\ T_{\alpha,i}^n & \text{if } G_{\alpha+1/2,i}^{k-1,n} < 0, \end{cases}$$

where the explicit quantity  $G_{\alpha+1/2,i}^{k-1,n}$  is computed using the previous estimation of the unknown quantities

$$\Delta t^n G_{\alpha+1/2,i}^{k-1,n} = \sum_{j=1}^{\alpha} \left[ l_j (\rho_{j,i}^{k-1,n} H_i^{k-1,n} - \rho_{j,i}^n H_i^n) + \sigma_i^n (F_{hj,i+1/2}^n - F_{hj,i-1/2}^n) \right].$$

The nonlinear problem (92) is solved for example by using a Newton-type algorithm. This is a small size problem but it has to be solved at each time step and for each cell  $C_i$ . In practice, this step is the most CPU time-consuming. Once  $H_i^{n+1}$  and  $T_{\alpha,i}^{n+1}$  are computed,  $u_{\alpha,i}^{n+1}$  is deduced from (61).

Let us remark that the Boussinesq assumption recalled in Sec. 2.2 simplifies significantly the numerical

scheme since in this case the density only appears in the wave velocity  $c_{\alpha,i}$ . Then we have

$$\tilde{X}_i^{n+1} = \begin{pmatrix} H_i^{n+1} \\ l_\alpha H_i^{n+1} u_{\alpha,i}^{n+1} \\ l_\alpha H_i^{n+1} T_{\alpha,i}^{n+1} \end{pmatrix},$$

and we easily recover the unknowns of interest without the solution of a nonlinear system. In fact the global water height  $H_i^{n+1}$  is explicitly defined by the sum of relations (60) and then quantities  $T_{\alpha,i}^{n+1}$  and  $u_{\alpha,i}^{n+1}$  can be computed using (61) and (63).

### 5.8. Stability of the scheme and maximum principle

Classically, the stability property of the kinetic scheme can be established through a CFL condition ensuring that the water height remains non negative. This CFL condition means that the quantity of water leaving a given cell during a time step  $\Delta t^n$  is less than the actual water in the cell. Note that due to the vertical discretization the water can leave the cell  $C_i$  of the layer  $\alpha$  either through the boundaries  $x_{i\pm 1/2}$ , or through the interfaces  $z_{\alpha\pm 1/2}$ . This makes the CFL condition more restrictive. In the case of a constant density, the resulting CFL constraint is given and demonstrated in [5]. Its adaptation to the situation where the density varies is straightforward and leads to the following proposition.

**Proposition 5.** *Assume that the function  $\chi$  has a compact support of length  $2w_M$ , then under the CFL condition*

$$\Delta t^n \leq \min_{1 \leq \alpha \leq N} \min_{i \in I} \frac{\rho_\alpha l_\alpha H_i^n \Delta x_i}{\rho_\alpha l_\alpha H_i^n (|u_{\alpha,i}^n| + w_M c_{\alpha,i}^n) + \Delta x_i \left( \left[ G_{\alpha+1/2,i}^{n+1/2} \right]_- + \left[ G_{\alpha-1/2,i}^{n+1/2} \right]_+ \right)}$$

the kinetic scheme defined in Sec. 5.2-5.7 keeps the water height positive, i.e.  $H_i^n \geq 0$  if this condition is true at initial time.

For the tracer concentration we have the two following propositions.

**Proposition 6.** *Under the CFL condition defined in Prop. 5, the kinetic scheme defined in Secs. 5.2-5.7 preserves the positivity of the tracer concentration.*

**Proof.** *We assume that  $T_{\alpha,i}^n \geq 0, \forall \alpha, i$  and we prove that  $T_{\alpha,i}^{n+1} \geq 0, \forall \alpha, i$ . We also assume that the CFL condition given in Prop. 5 is satisfied, so  $H_i^n \geq 0, \forall i$ .*

*From the positivity of the function  $\chi$  we deduce*

$$M_{\alpha,i}^n \geq 0, \quad \forall i, \quad \text{for } \alpha = 1, \dots, N.$$

*We now introduce the quantities*

$$[\xi]_+ = \max(0, \xi), \quad [\xi]_- = \max(0, -\xi).$$

*Using the definition of the Gibbs equilibrium  $U_\alpha$  (36), the definition (39) and the upwinding (77), we can write the upwind microscopic scheme (62) under the form*

$$\begin{aligned} g_{\alpha,i}^{n+1} &= (1 - \sigma_i^n |\xi|) U_{\alpha,i}^n + \sigma_i^n [\xi]_+ U_{\alpha,i-1}^n + \sigma_i^n [\xi]_- U_{\alpha,i+1}^n \\ &\quad + \Delta t^n \left( \left( \left[ V_{\alpha+1/2,i}^{n+1/2} \right]_+ - \left[ V_{\alpha+1/2,i}^{n+1/2} \right]_- \right) - \left( \left[ V_{\alpha-1/2,i}^{n+1/2} \right]_+ - \left[ V_{\alpha-1/2,i}^{n+1/2} \right]_- \right) \right), \\ &= (1 - \sigma_i^n |\xi|) T_{\alpha,i}^n M_{\alpha,i}^n + \sigma_i^n [\xi]_+ T_{\alpha,i-1}^n M_{\alpha,i-1}^n + \sigma_i^n [\xi]_- T_{\alpha,i+1}^n M_{\alpha,i+1}^n \\ &\quad + \Delta t^n \left( \left( T_{\alpha+1,i}^n \left[ N_{\alpha+1/2,i}^{n+1/2} \right]_+ - T_{\alpha,i}^n \left[ N_{\alpha+1/2,i}^{n+1/2} \right]_- \right) \right) \end{aligned}$$

$$\begin{aligned}
& - \left( T_{\alpha,i}^n \left[ N_{\alpha-1/2,i}^{n+1/2} \right]_+ - T_{\alpha-1,i}^n \left[ N_{\alpha-1/2,i}^{n+1/2} \right]_- \right) \\
= & T_{\alpha,i}^n \left( (1 - \sigma_i^n |\xi|) M_{\alpha,i}^n - \Delta t^n \left( \left[ N_{\alpha+1/2,i}^{n+1/2} \right]_- + \left[ N_{\alpha-1/2,i}^{n+1/2} \right]_+ \right) \right) \\
& \sigma_i^n [\xi]_+ T_{\alpha,i-1}^n M_{\alpha,i-1}^n + \sigma_i^n [\xi]_- T_{\alpha,i+1}^n M_{\alpha,i+1}^n \\
& + \Delta t^n \left( T_{\alpha+1,i}^n \left[ N_{\alpha+1/2,i}^{n+1/2} \right]_+ + T_{\alpha-1,i}^n \left[ N_{\alpha-1/2,i}^{n+1/2} \right]_- \right). \tag{93}
\end{aligned}$$

Since the quantity

$$\sigma_i^n |\xi| M_{\alpha,i}^n + \Delta t^n \left( \left[ N_{\alpha+1/2,i}^{n+1/2} \right]_- + \left[ N_{\alpha-1/2,i}^{n+1/2} \right]_+ \right),$$

represents, at the microscopic level, the water leaving the cell  $C_i$  of the layer  $\alpha$  during  $\Delta t^n$ , from Prop. 5 it satisfies

$$\int_{\mathbb{R}} \left( \sigma_i^n |\xi| M_{\alpha,i}^n + \Delta t^n \left( \left[ N_{\alpha+1/2,i}^{n+1/2} \right]_- + \left[ N_{\alpha-1/2,i}^{n+1/2} \right]_+ \right) \right) d\xi \leq \int_{\mathbb{R}} M_{\alpha,i}^n d\xi,$$

and we obtain

$$\rho_\alpha l_\alpha H_i^{n+1} T_{\alpha,i}^{n+1} = \int_{\mathbb{R}} g_{\alpha,i}^{n+1} d\xi \geq 0, \quad \forall i, \quad \text{for } \alpha = 1, \dots, N,$$

which completes the proof.  $\square$

**Proposition 7.** Under the CFL condition defined in Prop. 5, the kinetic scheme defined in Secs. 5.2-5.7 ensures a maximum principle for the tracer concentration. Indeed it satisfies

$$\forall n, \forall i, \forall \alpha \quad T_{\alpha,i}^{n+1} \leq \max\{T_{\alpha,i}^n, T_{\alpha+1,i}^n, T_{\alpha-1,i}^n, T_{\alpha,i+1}^n, T_{\alpha,i-1}^n\}.$$

**Proof.** From (93) using the CFL condition, we have

$$\begin{aligned}
g_{\alpha,i}^{n+1} & \leq \max\{T_{\alpha,i}^n, T_{\alpha+1,i}^n, T_{\alpha-1,i}^n, T_{\alpha,i+1}^n, T_{\alpha,i-1}^n\} \left( (1 - \sigma_i^n |\xi|) M_{\alpha,i}^n - \Delta t^n \left[ N_{\alpha+1/2,i}^{n+1/2} \right]_- - \Delta t^n \left[ N_{\alpha-1/2,i}^{n+1/2} \right]_+ \right. \\
& \quad \left. + \sigma_i^n [\xi]_+ M_{\alpha,i-1}^n + \sigma_i^n [\xi]_- M_{\alpha,i+1}^n + \Delta t^n \left[ N_{\alpha+1/2,i}^{n+1/2} \right]_+ + \Delta t^n \left[ N_{\alpha-1/2,i}^{n+1/2} \right]_- \right) \\
& = \max\{T_{\alpha,i}^n, T_{\alpha+1,i}^n, T_{\alpha-1,i}^n, T_{\alpha,i+1}^n, T_{\alpha,i-1}^n\} \tilde{f}_{\alpha,i}^{n+1},
\end{aligned}$$

with, using (58),

$$\int_{\mathbb{R}} \tilde{f}_{\alpha,i}^{n+1} d\xi = \int_{\mathbb{R}} f_{\alpha,i}^{n+1} d\xi.$$

Then, after an integration in  $\xi$  we obtain

$$\rho_\alpha l_\alpha H_i^{n+1} T_{\alpha,i}^{n+1} \leq \max\{T_{\alpha,i}^n, T_{\alpha+1,i}^n, T_{\alpha-1,i}^n, T_{\alpha,i+1}^n, T_{\alpha,i-1}^n\} \rho_\alpha l_\alpha H_i^{n+1},$$

which completes the proof.  $\square$

In practice, see [28], we rather introduce some upwinding in the tracer equation depending on the sign of the total mass flux. Then the tracer flux vanishes with the total mass flux. This is done with the introduction of the new tracer flux  $F_k(X_i, X_{i+1})$  defined in the following formula, which replaces (70):

$$F_{k_\alpha}(X_i, X_{i+1}) = T_{\alpha,i+1/2} F_{h_\alpha}(X_i, X_{i+1}),$$

where

$$T_{\alpha,i+1/2} = \begin{cases} T_{\alpha,i} & \text{for } F_{h_\alpha}(X_i, X_{i+1}) \geq 0, \\ T_{\alpha,i+1} & \text{for } F_{h_\alpha}(X_i, X_{i+1}) < 0. \end{cases} \tag{94}$$

Note that this upwinding technique preserves the properties demonstrated in the previous propositions.

### 5.9. Boundary conditions

The treatment of the boundary conditions is not detailed in this paper since it consists in a natural adaptation of the technique proposed by Bristeau and Coussin, see [29]. Note that for a given boundary, the type of prescribed condition – given water height, inflow, . . . – can vary depending on the considered layer.

### 5.10. Second order scheme

Second-order accuracy in time can be recovered by the Heun method [30], which is a modified version of the second order Runge-Kutta method. The advantage of the Heun scheme is that it preserves the invariant domains with no further restrictions on the CFL.

We also apply a formally second order scheme in space by a limited reconstruction of the variables [13]. These new variables are classically obtained with three ingredients: prediction of the gradients in each cell, linear extrapolation, and limitation procedure. The process is detailed in [27].

Note that the second order numerical scheme that we propose here does not adopt the same discretization for the pressure source terms as the method in [13] (not even for the case of a constant density single layer). Nonetheless the two approaches, the one presented here and the one in [13], give similar results and the convergence order of the schemes is the same (for smooth solutions). Nevertheless, our discretization of the topographic source term seems more natural, and for the second order extensions no additional centered source term is needed.

**Remark 5.1.** *In [13] the consistency and the existence of a semi-discrete in-cell entropy inequality for the scheme are demonstrated. The study of these two properties for the more general model that we propose here goes beyond the scope of this paper.*

## 6. Numerical results

In the case of constant density, the multilayer numerical model has been already validated, see [5]. In this section we focus on situations where the density variations have crucial influence on the hydrodynamical processes. First we illustrate the behavior of the proposed method in problems of non trivial static equilibria, then we show numerical experiments simulating flows exhibiting internal waves, and density-stratified water bodies subject to wind surface stress. The density is considered a function of the water temperature, see (11).

### 6.1. Static equilibria with non flat bottom

We illustrate here the properties of preservation of equilibria for stratified flows, see Sec. 5.6.

If we account for diffusion of the tracer, i.e.  $\mu_T \neq 0$  in relation (5), the only possible static equilibria are trivial and correspond to

$$\frac{\partial T}{\partial x} = Cst, \quad \text{and} \quad \frac{\partial T}{\partial z} = Cst, \quad \forall x, z, t.$$

To avoid these simplified situation, in the experiments of this section we set  $\mu_T = \nu_T = 0$ . Since our numerical scheme has small numerical dissipation, a Navier type bottom friction is considered in each simulation in order to reach static equilibrium more quickly.

We consider a 3 meter-long enclosed basin with vertical shores and an initial water level of  $H_0 + z_b = 1$  m, with the bottom geometry  $z_b(x)$  defined by the parabolic bump

$$z_b(x) = \max(-1, -0.75 - 1.246(x - 1.2)^2).$$

The computational grid has 100 nodes in the  $x$  direction.

In Figures 3 and 4 we illustrate the behavior of the scheme for two problems over non flat bottom with initial conditions corresponding to an unstable state.

For the first example, whose results are displayed in Fig. 3, the flow is initially at rest and the temperature distribution at  $t = t_0$  is defined as

$$T^0(x, z) = \begin{cases} 25^\circ\text{C} & \text{if } z - z_b \geq 2H_0/3, \\ 8^\circ\text{C} & \text{otherwise.} \end{cases}$$

For the simulation we have used a vertical discretization with 20 equally spaced layers, i.e.  $l_\alpha = 1/20$  for  $\alpha = 1, \dots, 20$ . The post-processing visualization tool performs a linear interpolation of the constant cell data, which explains the small diffusion of the temperature jump that is observed at the initial time. Figure 3-(b) shows that the system naturally reaches a stable equilibrium characterized by

$$\frac{\partial T}{\partial x} = 0.$$

In the second example, whose results are displayed in Fig. 4, we consider the same configuration as in the previous experiment but we set a different initial temperature distribution, which in this case deviates significantly from equilibrium conditions, see Fig. 4-(a). Also in this test the flow tends toward a stable static equilibrium state, see Fig. 4-(b).

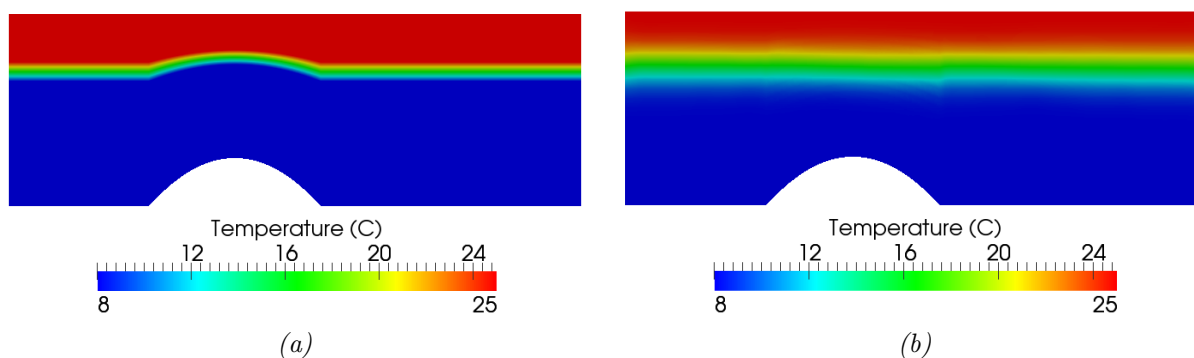


Figure 3: (a) initial state and (b) static equilibrium reached after 10 minutes.

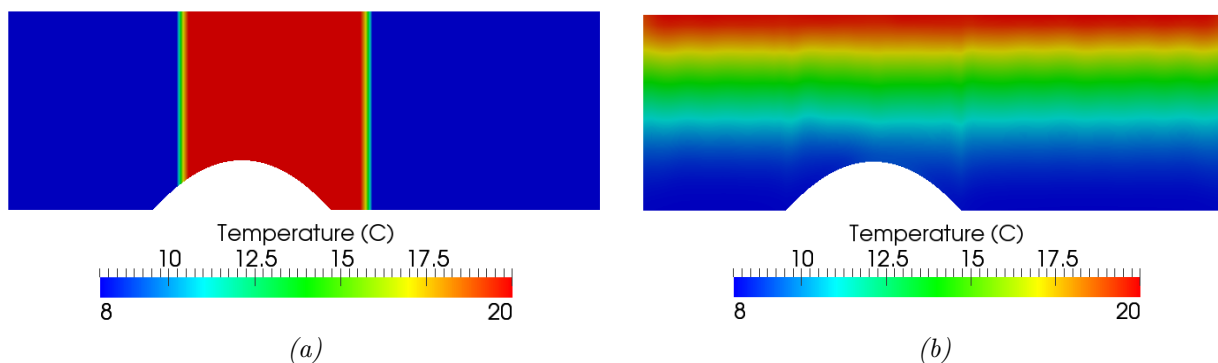


Figure 4: (a) initial state and (b) static equilibrium approximately reached after 20 minutes.

## 6.2. Internal gravity waves

In this section we present a test problem that shows that small numerical diffusivity is introduced by our numerical scheme.

Starting from an unstable initial condition, a stratified flow made of two miscible fluids asymptotically evolves, in presence of dissipative effects (fluid viscosity, tracer diffusivity, bottom friction), towards an equilibrium state that minimizes the potential energy  $E_p$  of the fluid volume  $V$ ,

$$E_p = \int_V \rho(T)gz \, dz,$$

and that corresponds to  $\frac{\partial T}{\partial x} = 0$ . Therefore the interface between the two fluids is asymptotically horizontal. This corresponds exactly to the situations depicted in Sec. 6.1 with Figs. 3 and 4.

In absence of physical diffusivity and friction, and still starting from an unstable initial condition, the potential energy has now no reason to decrease and interfacial gravity waves will appear in the fluid domain. The preservation of the interface between two miscible fluids for such gravity waves is a challenging task for numerical schemes, since in practice numerical diffusion coming from the scheme is often observed to lead to an artificial equilibrium in the simulations.

We refer in particular to [31] and references therein for numerical studies and simulations of interfacial gravity waves. In [31] various numerical schemes are compared with a test case corresponding to a finite amplitude deep-water standing wave. The interface is defined in [32] and given by

$$\zeta(x) = a \left( \left( 1 - \frac{(ka)^2}{64} \right) \cos kx - \frac{(ka)^2}{8} \cos 3kx \right),$$

where  $ka = 0.1$  is the initial steepness,  $k = 2\pi/L$ , and  $L$  is the length of the domain.

We perform here a test with the same configuration described in [31], where the interface thickness is  $k\delta = 0.01\pi$ . In Fig. 5 we show the profile of the density field at the initial time and after two periods of oscillation. The period of oscillation is  $T = 9.82$  seconds. We have used 80 nodes in the horizontal direction and 100 equally spaced layers in the vertical direction. Except near the interface where Fringer *et al.* [31] uses a refined mesh, our vertical computational grid corresponds to the one used in [31]. We see in Fig. 5-(b) that after two periods of oscillation we recover the initial shape of the interface  $\zeta$  even if some diffusion of the temperature is observed.

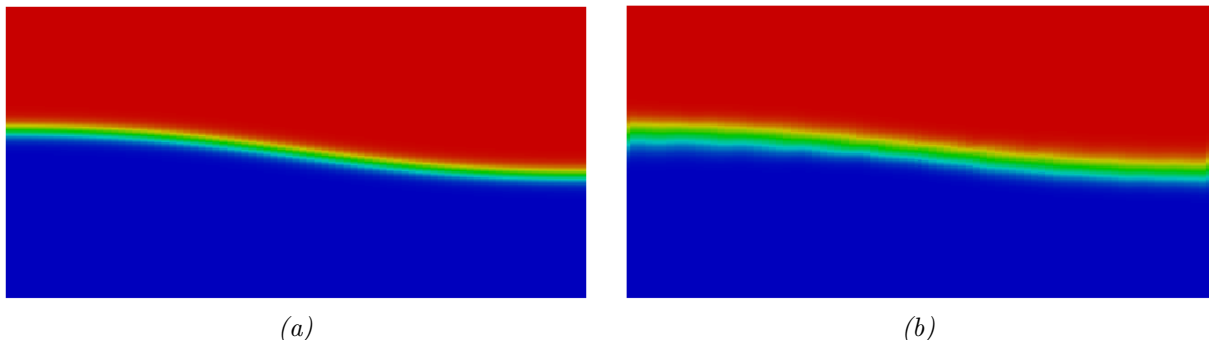


Figure 5: Density field for the interfacial standing wave, (a) initial condition and (b) after two periods of oscillation.

### 6.3. Validity of the Boussinesq assumption

In the literature the Boussinesq assumption (see Sec. 2.2) is very often considered, however its validity is sometimes unclear [33, 34]. As far as the authors know, most of the numerical schemes with validated results use this assumption, although there exist ocean models using various approximated versions of the non-Boussinesq equations [34]. It seems to the authors that the Boussinesq assumption is valid in the majority of the test problems they have simulated. However, in the case of internal waves in stratified flows and for long time simulations, the validity of the Boussinesq hypothesis is questionable. The following test case illustrates this point.

We consider the same geometry and initial conditions as in the first example of Sec. 6.1 and we compare in Figs. 6 the results that are obtained with and without the Boussinesq assumption. It appears that even if the system reaches in both situations the same static equilibrium condition (see Fig. 3-(b)), the transient velocity fields are different. The differences induced by the Boussinesq assumption in the simulations are reinforced, in our case, by the numerous reflections against the vertical shores. For an overview of the

physical situations where the Boussinesq assumption leads to significant errors, the reader can refer to [33, 34].

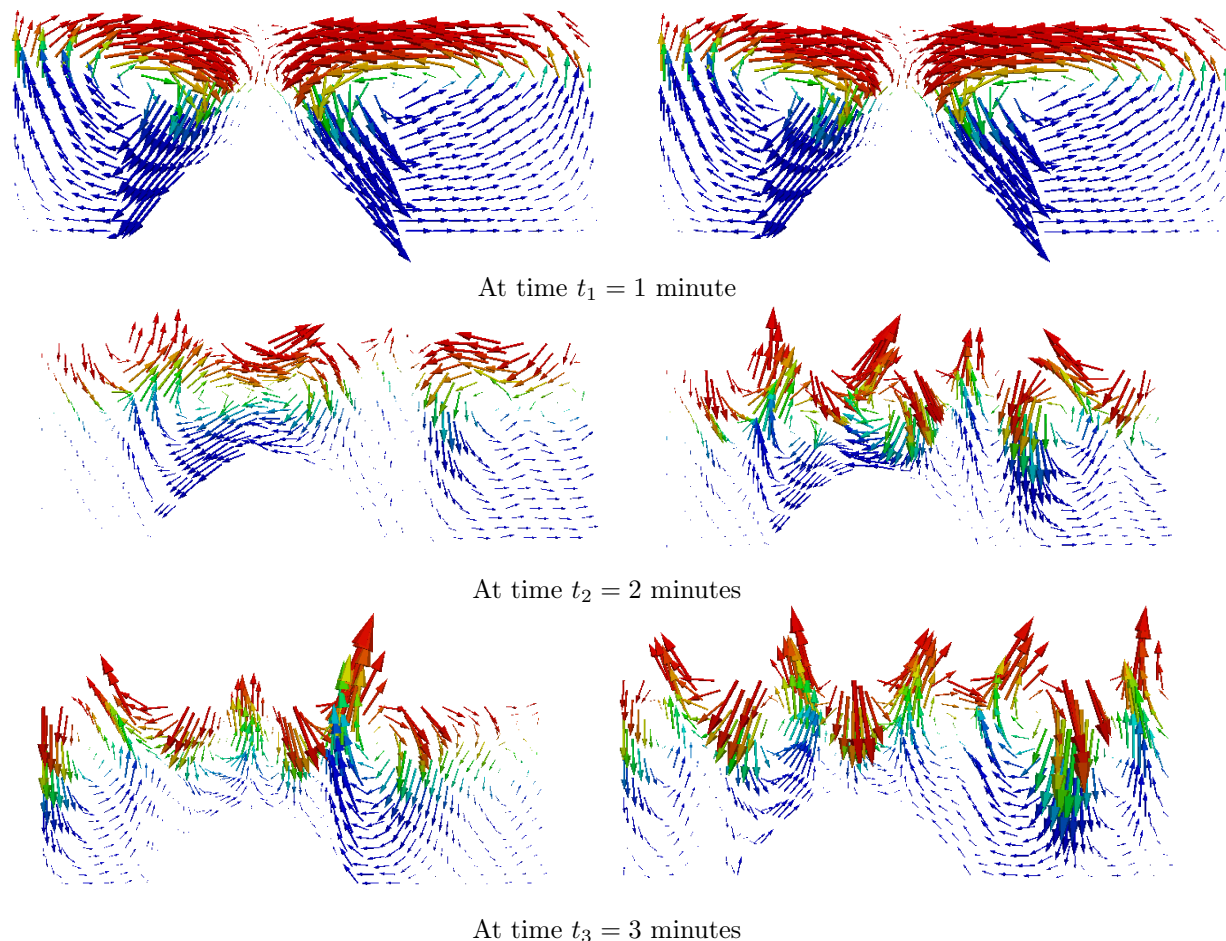


Figure 6: Computed velocity field. Left column: without the Boussinesq assumption; right column: with the Boussinesq assumption.

#### 6.4. Wind forced flows

We simulate in this section the response of a density-stratified water basin to wind stress. Thermo-hydrodynamical phenomena in lakes subject to the action of wind have been studied since a long time, by means of observations and measurements *in situ* [35, 36], laboratory experiments [36, 37, 38, 39], theoretical analysis [40, 41, 42], and, more recently, numerical simulations [43, 44, 3, 45].

The typical thermal stratification of natural lakes and hydraulic reservoirs consists of a warmer less dense surface layer, a colder denser bottom layer, and a middle layer characterized by a steep vertical thermal gradient, the center of which is the thermocline. Classically, in the literature the lake temperature distribution is schematized by a two-layer or three-layer thermal stratification.

When wind blows over these enclosed stratified water systems, the thermocline is deflected upward in the upwind region. The thermocline behaves as a barrier between an upper region with circular fluid motion that has the same direction as the wind at the surface, and a lower region with fluid rotating in the opposite sense. If the wind is sufficiently strong then the thermocline reaches the surface at the upwind end of the

basin and *upwelling* of colder fluid in the windward region occurs. This is quite different from the effect of wind forcing a homogeneous basin, where wind induces a simple circular motion of the fluid mass.

#### 6.4.1. Comparison with an analytical solution

In this section we simulate the steady setup of a two-layer flow subject to wind stress and we compare the results obtained through our numerical model with a local analytical solution. We consider a fluid in a rectangular basin of length  $L_b = 3$  m, and we impose a constant uniform wind stress from left to right at the free surface. The simulation starts with a flow at rest with the following two-layer temperature distribution (see Fig. 7):

$$T_0(x, z) = \begin{cases} 25^\circ\text{C} & \text{if } z - z_b \geq H_0/2, \\ 8^\circ\text{C} & \text{otherwise,} \end{cases} \quad (95)$$

where  $H_0 = 1$  m is the initial water height. Note that since at  $t_0 = 0$  we have

$$\frac{\partial \rho}{\partial z} \leq 0,$$

the initial state corresponds to a stable equilibrium. With these initial conditions, if wind is not too strong, the system is expected to reach the stationary regime described schematically in Fig. 7.

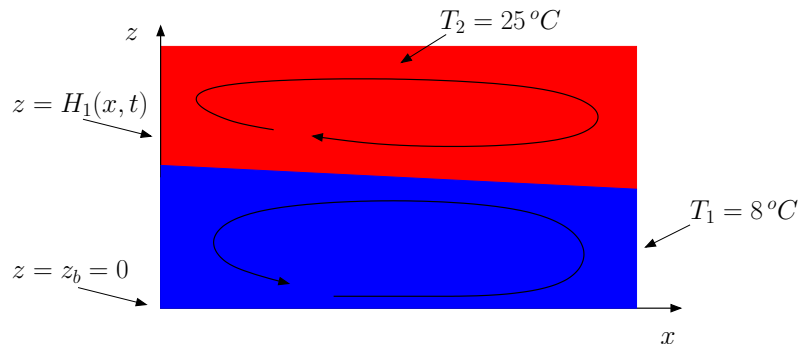


Figure 7: Steady setup of a two-layer flow subject to uniform and constant wind (from left to right). Flow domain with water height  $H(x, t)$  and layer interface  $H_1(x, t)$  (thermocline). At  $t_0$  we have  $H_1(x, t_0) = H_0/2$  and flow at rest. The steady configuration is characterized by deflections of opposite sign of the free surface and of the thermocline, and by opposite circulations in the upper and lower layer.

We use a viscosity  $\nu = 0.003 \text{ m}^2 \cdot \text{s}^{-1}$ , a Navier friction coefficient  $\kappa = 0.1 \text{ m} \cdot \text{s}^{-1}$  and a wind velocity of  $6 \text{ m} \cdot \text{s}^{-1}$  leading to  $a = -395.51$ ,  $\tilde{K} = 2.347 \text{ m} \cdot \text{s}^{-1}$ ,  $\alpha_1 = 3.63 \cdot 10^{-2} \text{ m}^2 \cdot \text{s}^{-1}$ ,  $\alpha_{1,0} = 8.63 \cdot 10^{-2} \text{ m}^2 \cdot \text{s}^{-1}$ ,  $\tau_w = 6.05 \cdot 10^{-5} \text{ m}^2 \cdot \text{s}^{-2}$  and  $\tau = 2.72 \text{ m}^2 \cdot \text{s}^{-2}$  in the formulas (A.5) and (A.6).

In agreement with the expected behavior, the results of the simulation show that the flow reaches a stationary configuration characterized by two circulation regions rotating in opposite sense below and above the thermocline. See the computed temperature distribution and vector velocity field at time  $t = 600$  s in Figure 8-(a). For this test problem, and also for the one considered in the next subsection 6.4.2, the shear stress due to the wind induces a gradient of the free surface. Nonetheless, the deflection of the free surface is very small, and it is not visible in the plots of the results (Figs. 8 and 10).

Additionally, we display in Figure 8-(b) the results obtained by performing a simulation with the same initial conditions of flow at rest and tracer distribution as in (95), but for the constant density case, that is we set  $\rho(T) = \rho_0$ . In such a situation we see that the wind induces a simple clockwise circular flow motion and a corresponding advection of the tracer  $T$ . In this case the flow velocity field attains a stationary rotating regime, but note that the only possible steady tracer distribution corresponds to the homogeneous conditions  $T(x, z, t) = \bar{T}$ . Let us also remark that for this test with constant density the convergence of the simulation results towards the analytical solution has already been investigated by the authors, see [5].

Note, moreover, that when the density variations are not considered the velocity profile along the vertical axis satisfies - far from the shores -

$$\frac{\partial^2 u}{\partial z^2} > 0,$$

whereas when the density variations are taken into account this quantity changes of sign when  $z$  varies from the bottom to the free surface. Because of the viscosity, the latter situation induces large dissipation and this explains why the velocities are smaller in Fig. 8-(a) (variable  $\rho$ ) than in Fig. 8-(b) ( $\rho = \rho_0$ ).

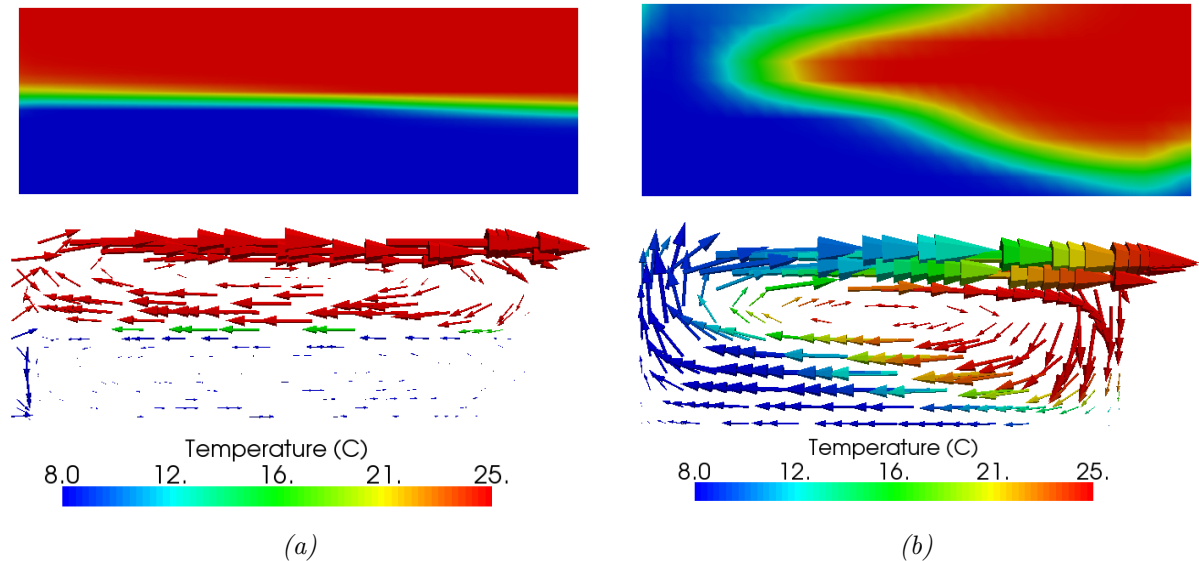


Figure 8: Computed temperature distribution and velocity field at time  $t = 600$  s. (a) Case of variable density,  $\rho(T) = \rho_0(1 - \alpha_T(T - T_0)^2)$ . The thermocline is tilted upward in the upwind region and two circulation regions appear. (b) Case of constant density,  $\rho(T) = \rho_0$ . A simple circular flow motion appears; in this case  $T$  is merely a tracer advected by the flow.

Under several simplifying hypotheses on the Navier–Stokes equations, for the steady stratified flow setup problem described above it is possible to derive an analytical solution for the horizontal velocity vertical profile at a position  $\bar{x}$  (far from basin ends) where the assumptions of vertical velocity  $w \approx 0$ , and  $\partial_x u \approx 0$ ,  $\partial_{xx} u \approx 0$  are reasonably satisfied. In particular, we consider as  $\bar{x}$  the mid-length of the lake. For the case of constant density, this analytical result is detailed in [46]. Here we extend the derivation of this local solution to the case of variable density, see Appendix A. Note that we have  $a < 0$  with  $|a| \gg 1$ , meaning that the deflection of the interface  $z = H_1$  is significantly larger in amplitude and has opposite sign with respect to the deflection of the free surface.

In Fig. 9-(a) we compare the analytical solution with the results obtained with the multilayer model for different vertical discretizations. Fig. 9-(a) presents the results obtained with 10, 30 and 50 discretization layers. For each computational grid the horizontal discretization is very fine, thus the error associated with this horizontal discretization is not relevant. We see in Fig. 9-(a) that our numerical results are in good agreement with the analytical solution.

In Fig. 9-(b) we display the rate of error versus the accuracy of the vertical discretization, namely the number of layers. The plot shows the  $\log(L^1 - \text{error})$  of the horizontal velocity at mid-length of the domain versus  $\log(h_0/h_i)$ . We denote by  $h_i$  the average cell height, while  $h_0$  is the average cell height of the coarser mesh. These error values have been computed on 5 grids with 5, 10, 20, 30 and 50 layers. It has to be noticed that, from (A.7),  $\frac{\partial H_1}{\partial x}$  is proportional to  $a$  and thus  $\frac{\partial H_1}{\partial x} < 0$ . Since the velocity at the interface is tangent to  $z = H_1$ , this means that we have  $w \neq 0$  near  $z = H_1$ , so the underlying assumption  $w \approx 0$  of

the analytical solution is not rigorously true. For these reasons, the analytical solution and the simulated velocity at mid-length of the basin are not completely consistent and the convergence rate appearing in Fig. 9-(b) is not completely meaningful.

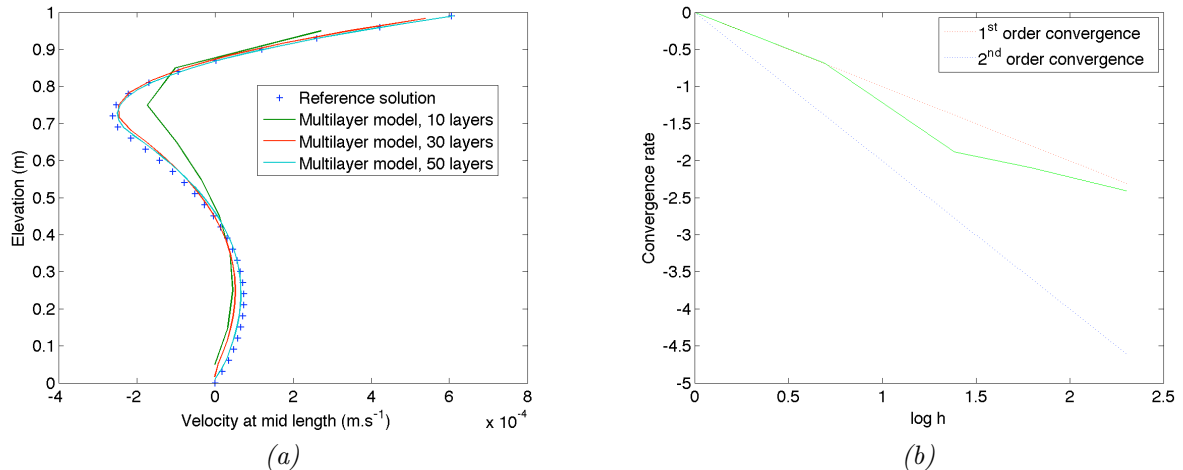


Figure 9: Comparison between analytical and computed velocities at mid-length of the basin.

#### 6.4.2. Upwelling

We now consider a test problem with the same configuration as the one in the previous section, but with a greater wind velocity. The domain is again a rectangular basin of length  $L_b = 3$  m, and we set an initial water height  $H_0 = 1$  m. The computational grid has 100 nodes in the  $x$  direction and 30 layers. The wind velocity (from left to right) is  $20 \text{ m} \cdot \text{s}^{-1}$ . We have used a viscosity  $\nu = \nu_T = 0.001 \text{ m}^2 \cdot \text{s}^{-1}$  and a Navier type bottom friction with  $\kappa = 0.1 \text{ m} \cdot \text{s}^{-1}$ . In Fig. 10 we show at different times the computed temperature distribution and the velocity field.

We observe, as expected, an upward deflection of the thermocline in the windward region (Fig. 10 at time  $t_1$ ), until it reaches the surface and upwelling of colder water occurs (Fig. 10 at time  $t_2$ ). Analogously to the experiment of the previous section (Fig. 8-(a)), two circulation regions appear above and below the thermocline, with opposite sense of rotation.

Due to the simplicity of our physical model (uniform diffusivity, hydrostatic pressure, lack of a turbulent mixing model), the aim of our numerical tests here is not attempting to reproduce realistic limnological processes on a long time scale. Rather, we emphasize the influence of density variations on the hydrodynamical response of the water body. In particular, the results of the simulations with variable density show that the numerical model is able to describe the tilting of the thermocline and upwelling of deeper fluid to the surface. Thus we are able to capture the essential features of the expected hydrodynamical behavior until the occurrence of upwelling. The post-upwelling flow dynamics cannot be modeled effectively by the present simplified model.

#### 6.5. A test case with dry areas, shocks and varying densities effects

In the previous numerical experiments we have considered situations with rather smooth solutions (low Froude number, small gradient of the free surface). However, in geophysical flows severe conditions and stiff processes may occur.

We conclude this section devoted to numerical results with a test case emphasizing the capability of our model to deal with dry areas, hydraulic jumps (shocks), and large and rapid variations of the free surface. We expect that for this type of problems our simulation tool offers superior performance with respect to

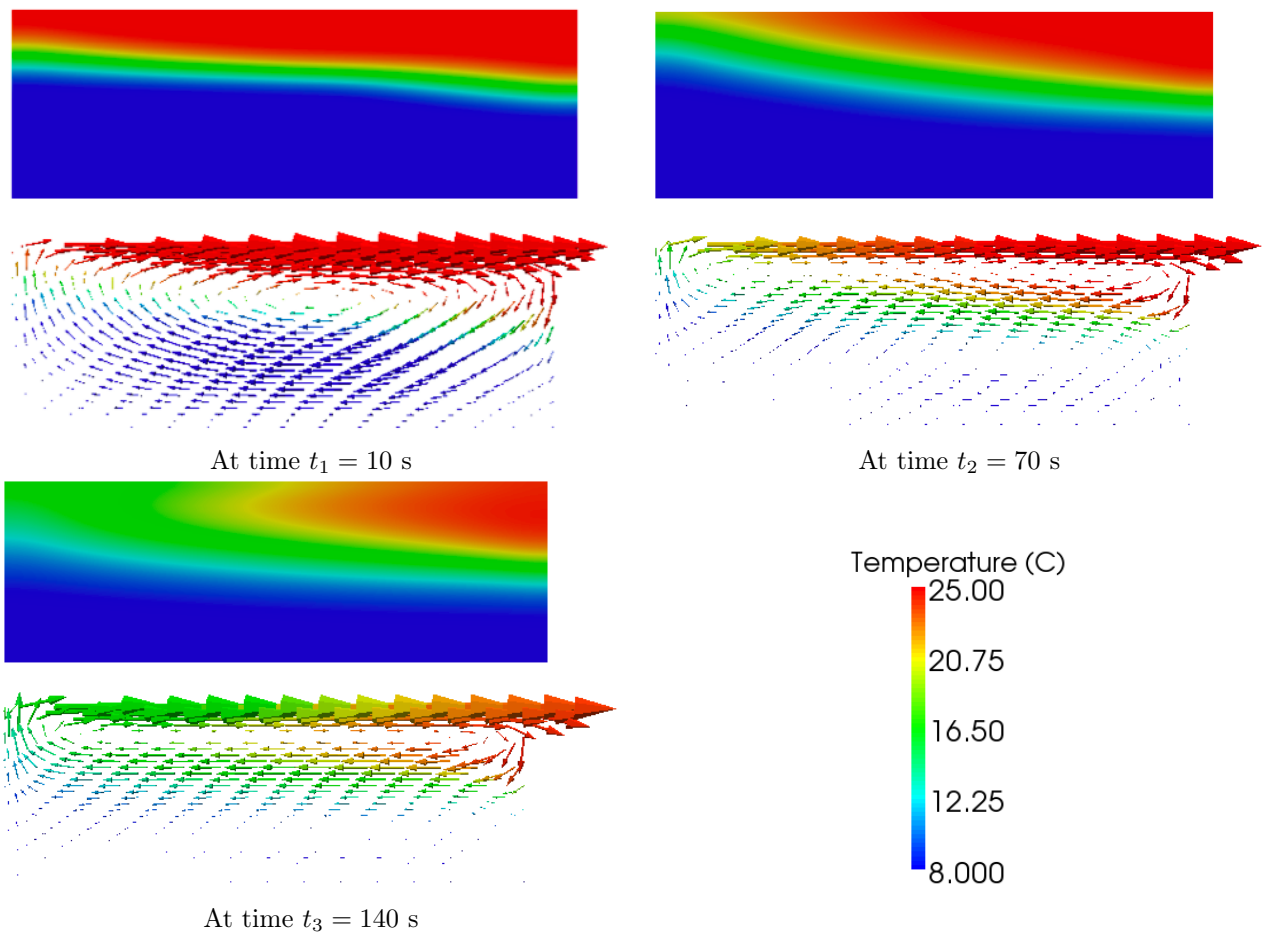


Figure 10: Temperature distribution and velocity field during the simulation of a simplified upwelling phenomenon. The three sub-figures display the tracer distribution and the velocity field at times  $t_1 = 10$  s,  $t_2 = 70$  s, and  $t_3 = 140$  s.

commonly used Navier–Stokes solvers, which, to our knowledge, would encounter difficulties in dealing with strong discontinuities and large free surface distortions of flows over variable topography with dry bed zones.

We consider a topography characterized by two bowl-shaped depressions, defined by

$$z_b(x) = -4e^{-0.1(x-10)^2} - 6e^{-0.2(x-18)^2},$$

for  $x \in [0, 25]$  m. The configuration and the initial conditions of the problem are depicted in Fig. 11. Initially the bowl on the left contains still cold water ( $T = 8^\circ\text{C}$ ), while the bowl on the right is filled with still hot water ( $T = 25^\circ\text{C}$ ). Moreover, at initial time a column of cold water ( $T = 8^\circ\text{C}$ ) sits on the plateau on the left of the first bowl, mimicking a dam-break initial condition. Simulation results at different times are shown in Fig. 12. At time  $t_1$  we observe the arrival of the fluid mass from the initial water column on the left in the first bowl with a discontinuity of the water depth. Because of the mass supply in the first bowl, and due to the dynamics induced by the water column, some cold water of the first bowl arrives in the second bowl filled with still hot water. Then the kinetic energy of this cold fluid arriving in the second bowl decreases, and it is no more able to compensate the Archimedes force to which is subject due to the pressure gradient induced by the temperature differences. At time  $t_4$  we see that the cold water in the second bowl begins to fall because of the Archimedes force.

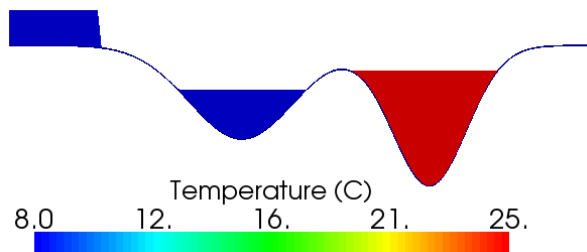


Figure 11: Initial conditions for the test case with dry areas, shocks and variable densities effects (section 6.5).

## 7. Conclusion

We have presented in this paper a new multilayer model with variable density for the simulation of density-stratified flows. The crucial distinguishing feature of our model with respect to classical multilayer approaches is its property of allowing inter-layer fluid circulation. The numerical method for the system solution is based on a kinetic interpretation of the model, which allows building a stable positivity preserving scheme. Well-balancing of source terms is obtained through an extended hydrostatic reconstruction technique, and the resulting scheme is formally second-order accurate. Numerical results show the ability of the multilayer model to correctly capture the hydrodynamical behavior of stratified flows related to density gradients effects.

Work is in progress to include in the present model non-hydrostatic terms, following the studies of the authors in [47]. In the future, we plan to take into account additional physical phenomena, in particular surface thermodynamics and turbulent mixing.

**Acknowledgements.** The work of the third author (M. Pelanti) has been supported by *Électricité de France* (INRIA-EDF collaborative research contract n. 8610-APP-5910049348). The authors would like to thank Benoît Perthame and Marie-José Salençon for valuable suggestions and precious assistance in these studies.

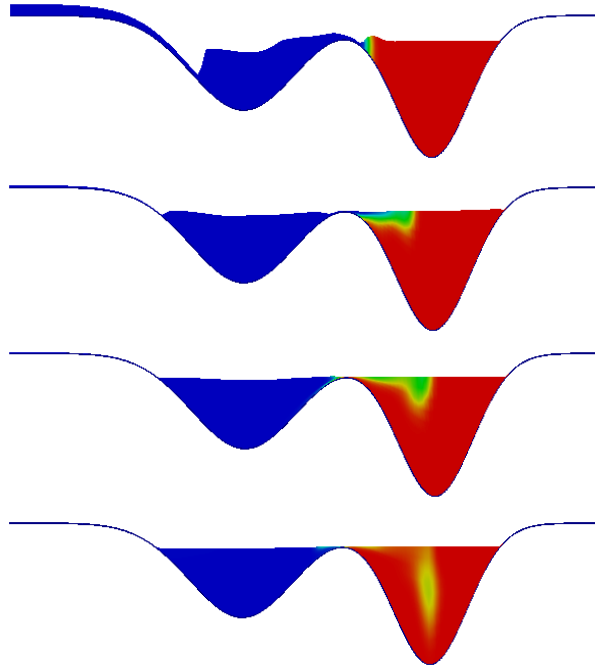


Figure 12: Flow dynamics at four different times,  $t_1 = 2.5$  s,  $t_2 = 7.5$  s,  $t_3 = 12.5$  s, and  $t_4 = 27.5$  s (plots from top to bottom).

## References

- [1] D. Beletsky, W. P. O'Connor, D. J. Schwab, D. E. Dietrich, Numerical simulation of internal Kelvin waves and coastal upwelling fronts, *J. Phys. Oceanogr.* 27 (1997) 1197–1215.
- [2] V. Casulli, A semi-implicit finite difference method for non-hydrostatic, free-surface flows, *Internat. J. Numer. Methods Fluids* 30 (1999) 425–440.
- [3] R. Hodges, J. Imberger, A. Saggio, K. B. Winters, Modeling basin-scale internal waves in a stratified lake, *Limnol. Oceanogr.* 45 (2000) 1603–1620.
- [4] J.-M. Hervouet, *Hydrodynamics of Free Surface Flows: Modelling with the Finite Element Method*, Wiley, 2007.
- [5] E. Audusse, M.-O. Bristeau, B. Perthame, J. Sainte-Marie, A multilayer Saint-Venant system with mass exchanges for Shallow Water flows. Derivation and numerical validation., *ESAIM: M2AN* (published on line) (2010).
- [6] A.-J.-C. Barré de Saint-Venant, Théorie du mouvement non permanent des eaux avec applications aux crues des rivières et à l'introduction des marées dans leur lit, *C. R. Acad. Sci. Paris* 73 (1871) 147–154.
- [7] L. V. Ovsiannikov, Two-layer shallow water models, *Prikl. Mekh. Tekh. Fiz.* 2 (1979) 3–14.
- [8] C. B. Vreugdenhil, Two-layer shallow-water flow in two dimensions, a numerical study, *J. Comput. Phys.* 33 (1979) 169–184.
- [9] M.-J. Castro, J. Macías, C. Parés, A Q-scheme for a class of systems of coupled conservation laws with source term. application to a two-layer 1-D shallow water system., *M2AN Math. Model. Numer. Anal.* 35 (2001) 107–127.
- [10] F. Bouchut, V. Zeitlin, A robust well-balanced scheme for multi-layer shallow water equations, *Discrete Contin. Dyn. Syst. Ser. B* 13 (2010) 739–758.
- [11] A. Decoene, J.-F. Gerbeau, Sigma transformation and ALE formulation for three-dimensional free surface flows., *Internat. J. Numer. Methods Fluids* 59 (2009) 357–386.
- [12] B. Perthame, C. Simeoni, A kinetic scheme for the Saint-Venant system with a source term, *Calcolo* 38 (2001) 201–231.
- [13] E. Audusse, F. Bouchut, M.-O. Bristeau, R. Klein, B. Perthame, A fast and stable well-balanced scheme with hydrostatic reconstruction for Shallow Water flows, *SIAM J. Sci. Comput.* 25 (2004) 2050–2065.
- [14] F. Bouchut, *Nonlinear stability of finite volume methods for hyperbolic conservation laws and well-balanced schemes for sources*, Birkhäuser, 2004.
- [15] R. Bleck, L. T. Smith, A wind-driven isopycnic coordinate model of the North and Equatorial Atlantic Ocean; 1. Model development and supporting experiments., *J. Geophys. Res.* 95 (1990) 3273–3285.
- [16] R. Hallberg, Some aspects of the circulation in ocean basins with isopycnals intersecting the sloping boundaries, Ph.D. thesis, University of Washington, 1995.
- [17] A. Etemad-Shahidi, J. Imberger, Diapycnal mixing in the thermocline of lakes: Estimations by different methods, *Environmental Fluid Mechanics* 6 (2006) 227–240.

- [18] P.-L. Lions, *Mathematical Topics in Fluid Mechanics. Vol. 1: Incompressible models.*, Oxford University Press, 1996.
- [19] J. Imberger, *Physical Processes in Lakes and Oceans*, American Geophysical Union, 1998.
- [20] J.-F. Gerbeau, B. Perthame, Derivation of Viscous Saint-Venant System for Laminar Shallow Water; Numerical Validation, *Discrete Contin. Dyn. Syst. Ser. B* 1 (2001) 89–102.
- [21] F. Marche, Derivation of a new two-dimensional viscous shallow water model with varying topography, bottom friction and capillary effects, *European Journal of Mechanics /B* 26 (2007) 49–63.
- [22] F. Bouchut, M. Westdickenberg, Gravity driven shallow water models for arbitrary topography, *Comm. in Math. Sci.* 2 (2004) 359–389.
- [23] B. Mohammadi, O. Pironneau, F. Valentin, Rough boundaries and wall laws, *Internat. J. Numer. Methods Fluids* 27 (1998) 169–177.
- [24] J. Sainte-Marie, Vertically averaged models for the free surface Euler system. Derivation and kinetic interpretation., Accepted for publication in *M3AS* (2010).
- [25] B. Perthame, *Kinetic formulation of conservation laws.*, Oxford University Press, 2002.
- [26] E. Audusse, M.-O. Bristeau, A. Decoene, Numerical simulations of 3d free surface flows by a multilayer Saint-Venant model, *Internat. J. Numer. Methods Fluids* 56 (2008) 331–350.
- [27] E. Audusse, M.-O. Bristeau, A well-balanced positivity preserving second-order scheme for shallow water flows on unstructured meshes., *J. Comput. Phys.* 206 (2005) 311–333.
- [28] E. Audusse, M.-O. Bristeau, Transport of pollutant in shallow water flows : A two time steps kinetic method, *ESAIM: M2AN* 37 (2003) 389–416.
- [29] M. Bristeau, B. Coussin, Boundary Conditions for the Shallow Water Equations solved by Kinetic Schemes, Research Report RR-4282, INRIA, 2001.
- [30] F. Bouchut, An introduction to finite volume methods for hyperbolic conservation laws., *ESAIM Proc.* 15 (2004) 107–127.
- [31] O.-B. Fringer, S.-W. Armfield, R.-L. Street, Reducing numerical diffusion in interfacial gravity wave simulations., *Int. J. Num. Meth. Fluids.* 49 (2005) 301–329.
- [32] S.-A. Thorpe, On standing internal waves of finite amplitude., *J. Fluid Mech.* 32 (1968) 299–319.
- [33] T. J. McDougall, R. J. Greatbatch, Y. Lu, On conservation equations in oceanography: How accurate are Boussinesq ocean models?, *Journal of Physical Oceanography* 32 (2002) 1574–1584.
- [34] R.-J. Greatbatch, Y. Lu, Y. Cai, Relaxing the Boussinesq approximation in ocean circulation models, *Journal of Atmospheric and Oceanic Technology* 18 (2001) 1911–1923.
- [35] E. M. Wedderburn, Temperature observations in Loch Earn, with a further contribution to the hydrodynamical theory of the temperature seiche, *Trans. R. Soc. Edin.* 48 (1912) 629–695.
- [36] C. H. Mortimer, Water movements in lakes during summer stratification; evidence from the distribution of temperature in Windermere, *Phil. Trans. R. Soc. B* 236 (1952) 255–404.
- [37] C. Kranenburg, Mixed-layer deepening in lakes after wind set-up, *J. Hydraul. Div. ASCE* 111 (1985) 334–354.
- [38] S. G. Monismith, An experimental study of the upwelling response of stratified reservoirs to surface shear stress, *J. Fluid Mech.* 171 (1986) 407–439.
- [39] C. Stevens, J. Imberger, The initial response of a stratified lake to a surface shear stress, *J. Fluid Mech.* 312 (1996) 39–66.
- [40] N. S. Heaps, A. E. Ramsbottom, Wind effects on water in a narrow two-layered lake, *Phil. Trans. R. Soc. London A* 312 (1966) 391–430.
- [41] S. G. Monismith, Wind-forced motions in stratified lakes and their effect on mixed-layer shear, *Limnol. Oceanogr.* 30 (1985) 771–783.
- [42] J. Imberger, J. C. Patterson, Physical limnology, *Adv. Applied Mech.* 27 (1990) 303–475.
- [43] R. O. R. Y. Thomsson, J. Imberger, Response of a numerical model of a stratified lake to wind stress, in: T. Carsten, T. McClimans (Eds.), *Second International Symposium on Stratified Flows*, IAHR, Trondheim, Norway, pp. 562–570.
- [44] C. R. Chu, C. K. Soong, Numerical simulation of wind-induced entrainment in a stably stratified water basin, *J. Hydraul. Research IAHR* 35 (1997) 21–41.
- [45] P. Okely, J. Imberger, Horizontal transport induced by upwelling in a canyon-shaped reservoir, *Hydrobiologia* 586 (2007) 343–355.
- [46] N. J. Shankar, H. F. Cheong, S. Sankaranarayanan, Multilevel finite-difference model for three-dimensional hydrodynamic circulation, *Ocean Engineering* 24 (1997) 785–816.
- [47] M.-O. Bristeau, J. Sainte-Marie, Derivation of a non-hydrostatic shallow water model; Comparison with Saint-Venant and Boussinesq systems, *Discrete Contin. Dyn. Syst. Ser. B* 10 (2008) 733–759.

## Appendix A. Local analytical solution for a two-layered flow subject to wind stress

We start with the two-dimensional hydrostatic Navier–Stokes system (1)–(5), with the initial conditions and the notations defined in Fig. 7. Since we have a two-layered basin, the density can be written:

$$\rho(z) = \rho_1 + (\rho_2 - \rho_1)H_e(z - H_1), \quad (\text{A.1})$$

where  $H_e$  is the Heaviside function and  $\rho_i = \rho(T_i)$  for  $i = 1, 2$ .

We look for the stationary solution of this problem, by assuming  $\nu_T = 0$ , and by considering a vertical

viscosity only for the  $x$ -momentum equation. Near the mid-length of the basin we can assume

$$\frac{\partial u}{\partial x} \approx 0, \quad \text{and} \quad w \approx 0. \quad (\text{A.2})$$

Therefore, in this region, the stationary solution of the system (1)-(3), (5), neglecting nonlinear convective terms, satisfies

$$\nu \frac{\partial^2 u}{\partial z^2} - g \frac{\partial}{\partial x} \int_z^\eta \rho(T) dz = 0. \quad (\text{A.3})$$

By using (A.1) in the equilibrium condition above, we obtain

$$\nu \frac{\partial^2 u}{\partial z^2} - g \rho_2 \frac{\partial H}{\partial x} - g(\rho_1 - \rho_2) \frac{\partial H_1}{\partial x} H_e(H_1 - z) = 0. \quad (\text{A.4})$$

Let  $\tau_w$  and  $\tau_b$  denote respectively the shear stress at the free surface (wind stress) and at the bottom (Navier friction). A first integration of (A.4) from  $z_b$  to  $z$  gives

$$\begin{aligned} \nu \frac{\partial u}{\partial z} - \tau_b &= \rho_2 g(z - z_b) \frac{\partial H}{\partial x} + (\rho_1 - \rho_2) g(z - z_b) \frac{\partial H_1}{\partial x} H_e(H_1 - z) \\ &\quad + (\rho_1 - \rho_2) g H_1 \frac{\partial H_1}{\partial x} H_e(z - H_1), \end{aligned}$$

and a second integration from  $z_b$  to  $z$  gives

$$\begin{aligned} \nu(u - u_b) &= (z - z_b) \tau_b + \frac{\rho_2 g}{2} (z - z_b)^2 \frac{\partial H}{\partial x} \\ &\quad + g(\rho_1 - \rho_2) \frac{\partial H_1}{\partial x} \left( \frac{(z - z_b)^2}{2} H_e(H_1 - z) + H_1 \left( z - \frac{H_1}{2} \right) H_e(z - H_1) \right). \end{aligned}$$

Then, the mass conservation condition in the layer where  $T = T_1$  gives

$$-\nu u_b = \frac{H_1}{2} \tau_b + \frac{\rho_2 g}{6} H_1^2 \frac{\partial H}{\partial x} + \frac{(\rho_1 - \rho_2) g}{6} H_1^2 \frac{\partial H_1}{\partial x},$$

while mass conservation in the layer where  $T = T_2$  leads to

$$-\nu u_b = \frac{H + H_1}{2} \tau_b + \frac{\rho_2 g}{6} (H^2 + H H_1 + H_1^2) \frac{\partial H}{\partial x} + (\rho_1 - \rho_2) g \frac{H_1}{2} \frac{\partial H_1}{\partial x}.$$

From the two previous relations, since we have a Navier type friction law at the bottom, i.e.  $\tau_b = \kappa u_b$ , we obtain

$$u_b = -\frac{1}{\alpha_1} \left( \frac{\rho_2 g}{6} H_1^2 \frac{\partial H}{\partial x} + \frac{(\rho_1 - \rho_2) g}{6} H_1^2 \frac{\partial H_1}{\partial x} \right) \quad (\text{A.5})$$

$$(\rho_1 - \rho_2) \left( \frac{H_1^2}{6\alpha_1} - \frac{H_1 H}{2\alpha_{1,0}} \right) \frac{\partial H_1}{\partial x} = \frac{\rho_2}{6} \left( \frac{H^2 + H H_1 + H_1^2}{\alpha_{0,1}} - \frac{H_1^2}{\alpha_1} \right) \frac{\partial H}{\partial x}, \quad (\text{A.6})$$

with  $\alpha_1 = \nu + \kappa H_1/2$ ,  $\alpha_{1,0} = \nu + \kappa(H + H_1)/2$ . Now, integration of (A.4) from  $z_b$  to  $\eta$  gives

$$\tau_w - \kappa u_b = \rho_2 g H \frac{\partial H}{\partial x} + (\rho_1 - \rho_2) g H_1 \frac{\partial H_1}{\partial x}.$$

Hence, with obvious notations, we finally have

$$\frac{\partial H_1}{\partial x} = a \frac{\partial H}{\partial x}, \quad u_b = \tilde{K} \frac{\partial H}{\partial x}, \quad \tau_w = \tau \frac{\partial H}{\partial x}, \quad (\text{A.7})$$

and

$$\begin{aligned} u(z) &= \left( \tilde{K} + \kappa \tilde{K} \frac{z - z_b}{\nu} + \frac{\rho_2 g}{2\nu} (z - z_b)^2 + \frac{(\rho_1 - \rho_2)g}{2\nu} a(z - z_b)^2 H_e(H_1 - z) \right. \\ &\quad \left. + \frac{(\rho_1 - \rho_2)g}{\nu} a H_1 \left( z - \frac{H_1}{2} \right) H_e(z - H_1) \right) \frac{\tau_w}{\tau}. \end{aligned}$$